Runoff Forecast and Analysis of the Probability of Dry and Wet Transition in the Hanjiang River Basin

Haoyu Jin
Sun Yat-sen University
Xiaohong Chen (Eescxh@Mail.sysu.edu.cn)
Sun Yat-sen University
Ruida Zhong
Sun Yat-sen University

Research Article

Keywords: Runoff forecast, trend analysis, Markov chain, dry and wet conversion

Posted Date: June 9th, 2021

DOI: https://doi.org/10.21203/rs.3.rs-576486/v1

Runoff forecast and analysis of the probability of dry and wet transition in the Hanjiang River Basin

Haoyu Jin [1, 2, 3] · Xiaohong Chen [1, 2, 3, *], Ruida Zhong [1, 2, 3]

Received: Date/ Accepted: Date

Abstract

Runoff prediction has an important guiding role in the planning and management of regional water resources, flood prevention and drought resistance, and can effectively predict the risk of changes in regional water resources. This study used 12 runoff prediction methods to predict the runoff of four hydrological stations in the Hanjiang River Basin (HRB). Through the MCMC method, the HRB runoff probability conversion model from low to high (high to low) is constructed. The study found that the runoff of the HRB had a decreasing trend. In the mid-1980s, the runoff had a significant decreasing trend. The smoother the runoff changes, the easier it is to make accurate prediction. On the whole, the QS-MFM, MFM, MA-MFM, CES and DNN methods have strong generalization ability and can more accurately predict the runoff of the HRB. The Logistic model can accurately simulate the change of runoff status in the HRB. Among them, the HLT station has the fastest conversion rate of drought and flood, and the flow that generates floods is 6 times that of drought. The smaller the basin area, the larger the gap between drought and flood discharge. Overall, this research provides important technical support for the prediction of change in water resources and the transition probability from drought to flood in the HRB.

Key words: Runoff forecast · trend analysis · Markov chain · dry and wet conversion

1 Introduction

Although affected by the fluctuation of global climate circulation, the regional climate environment has certain stability and continuity(Li et al., 2021; Nygren et al., 2020; Yaduvanshi et al., 2021). Finding the law from the long-term runoff time series to extend the runoff time series can effectively predict the changes of regional water resources and provide references for the rational use of water resources and the prediction of droughts and floods(Ma et al., 2020; Shappell et al., 2021; Tian et al., 2018; Turunen et al., 2020). Due to rapid population growth, economic and social development, regional water consumption continues to rise(Deng et al., 2020; Dong et al., 2021; Ferrucci and Vocciante, 2021). In northern China, water shortages have become a major factor restricting regional economic and social development(Cheng et al., 2019; Li et al., 2017). At the same time, the South-to-North Water Diversion Project transfers water from the south to the north, which increases the risk in water resources

[1] Center for Water Resources and Environment, Sun Yat-sen University, Guangzhou 510275, China
[2] Guangdong Engineering Technology Research Center of Water Security Regulation and Control for Southern China, Sun Yat-sen University, Guangzhou 510275, China
[3] Key Laboratory of Water Cycle and Water Security in Southern China of Guangdong High Education Institute, Sun Yat-sen University, Guangzhou 510275, China
* Corresponding author. E-mail address: eescxh@mail.sysu.edu.cn (X. Chen).

in the southern water diversion area to a certain extent(Feng et al., 2011; Guo et al., 2020; Qu et al., 2020; Yu et al., 2020). Therefore, the short-medium term prediction of water resources can provide reference significance for the formulation of reasonable economic and social development plans for the region(Chen et al., 2020; Wang et al., 2015; Xie et al., 2019).

Hydrological forecasting has always been a major issue of concern(Piotrowski and Napiorkowski, 2012). At present, the commonly used methods of hydrological forecasting include physical cause analysis methods, mathematical statistics, intelligent algorithms, and comprehensive forecasting methods based on numerical weather prediction(Badrzadeh et al., 2015; Liu, 2014; Ouyang et al., 2007; Pan and Wang, 2004). However, due to the interaction and mutual influence of many factors, river runoff shows significant nonlinearity, high-dimensionality, chaos, ambiguity and many other complex features, which affects the prediction accuracy of the above methods to varying degrees(Moosavi et al., 2017; Wu, 2018; Xiu-fen et al., 2003). So far, no single method has absolute advantages, and runoff time series with different characteristics are suitable for different forecasting methods(Löwe et al., 2014). The mathematical statistics method is relatively simple. It is to find the change rule on the original time series and then make a reasonable extension of the series(Chua and Wong, 2011; He et al., 2020). The prediction method based on the background of the weather system requires analysis of the climate condition. Although the prediction accuracy is high, it increases the complexity of the prediction(Archer and Fowler, 2008; Doycheva et al., 2017). In recent years, deep neural network algorithms have shown superior performance in regression prediction and have also been widely used in hydrological prediction(Ghumman et al., 2011; Parida et al., 2006; Sedki et al., 2009).

The Han River is the largest tributary of the Yangtze River, the main water source in the Jianghan Plain, and the water source for the Middle Route of the South-to-North Water Diversion Project(Qi et al., 2020). This study used a variety of prediction methods to predict the runoff of the four hydrological stations in the HRB and compared the advantages and disadvantages of different methods. On this basis, the conversion mechanism of drought and flood in the basin was analyzed by Markov chain Monte Carlo method. It provides reference significance for the prediction of water resources in the HRB and the forecast of drought and flood disasters.

2 Methods and data

2.1 Study area and data

The Han River is the largest tributary of the Yangtze River Basin, with a total length of more than 1,500 kilometers and a drainage area of 159,000 km²(Yang et al., 2021). The climate of the HRB (106°12′-114°14′E, 30°08′-34°11′N) has obvious characteristics of subtropical monsoon climate. The climate is relatively mild, with an average annual temperature between 15-17 ℃. Rainfall in the Han River Basin is relatively abundant, with an average annual rainfall of 600-1300 mm. The precipitation is mainly

concentrated in the summer half year, accounting for more than 70% of the annual precipitation(Zhou et al., 2017). Among them, June, July, and August are particularly prominent, with precipitation accounting for about 40%-50% of the annual total. The main source of the water volume of the Han River and its tributaries is rainwater, followed by groundwater. Groundwater recharge accounts for about 15-20% of the annual runoff. Therefore, the annual runoff changes of the rivers in the Han River system are basically the same as the annual precipitation changes. The runoff varies greatly from year to year in the basin. The maximum annual runoff is generally more than three times the size of the minimum annual runoff. The annual average runoff of the whole basin is about 60 billion cubic meters. Due to abundant rainfall, water resources in the basin are very abundant. However, there are differences in the distribution of water resources in the basin and uneven seasonal distribution, and water needs to be transferred outside the basin. There has been a decreasing trend in water resources in recent years.

Fig. 1 illustrates the topography, water system and hydrological station distribution of the Han River Basin. It can be seen from the figure that the topography of the Han River Basin is high in the west and low in the east, with dense river networks. The hydrological stations are distributed in the upper, middle and lower reaches. Except for Huanglongtan (HLT) station, which is on the tributary Zenghe, Baihe (BH) station, Huangjiagang (HJG) station, and Huangzhuang (HZ) stations are all on the main stream. This study used flow data from four hydrological stations from 1960 to 2014.

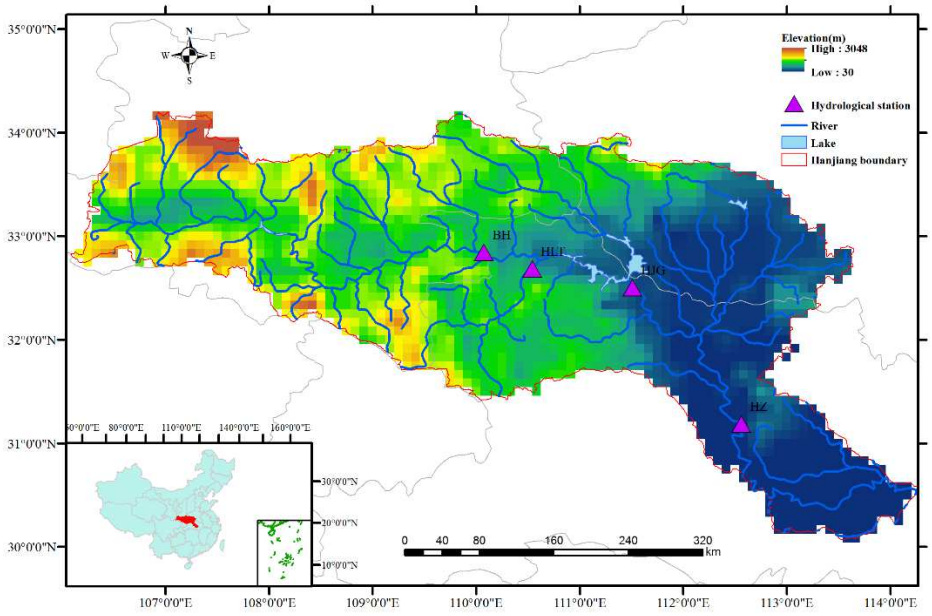

Fig. 1 Topography of the study area and distribution of the hydrological stations

2.2 Methods

2.2.1 ARIMA and SARIMA

Time series refers to a series of numbers of the same statistical indicator in the order of their occurrence. The main purpose of time series analysis is to predict the future based on historical data. There are four commonly used time series models: Autoregressive model (AR(p)), Moving average model (MA(q)), Autoregressive moving average model (ARMA(p, q)), and Autoregressive Integrated Moving Average model (ARIMA(p, d, q)). It can be said that the first three are special forms of the ARIMA(p, d, q) model(Khan et al., 2020). The ARIMA model is established on the basis of a stationary time series, so the stationarity of the time series is an important prerequisite for modeling. The method of testing the stability of the time series model generally employs the ADF unit root test model. Of course, if the time series is unstable, it can be turned stable through certain operations (such as taking the logarithm, difference), and then the ARIMA model is performed to obtain stable time series forecast results. Finally, the inverse operation is performed on the prediction results (such as the inverse operation of the difference) to get the prediction results of the original data. The ARIMA model can be expressed as follows:

$$\left(1-\sum_{i=1}^{p}\phi_i L^i\right)(1-L)^d X_t = \left(1+\sum_{i=1}^{q}\theta_i L^i\right)\varepsilon_t \quad (1)$$

Where L is the lag operator, p is the betweenness of the autoregressive process, d is the betweenness of the difference, and q is the betweenness of the moving average process. ϕ is the parameter of the autoregressive part of the model, X is the time series, θ is the parameters of the moving average part, and ε is the error term.

The Seasonal Autoregressive Integrated Moving Average (SARIMA) model adds seasonal factors on the basis of the ARIMA model and is suitable for unstable data with trend cycles(Carmona-Benítez and Nieto, 2020). In addition to seasonal changes, this cycle can also be caused by other factors.

2.2.2 Exponential smoothing method

The exponential smoothing method is a special weighted moving average method, which strengthens the effect of recent observations on the predicted value. The weights assigned to the observations at different times are not equal, and the weight of the recent observations is increased, which can change the changing rate of the curve according to the weight coefficient. It does not abandon the past data, and only imposes a gradually weakening degree of influence, that is, as the data moves away, it gives a weight that gradually converges to zero. It is a time series-based forecasting method, which is generally divided into single exponential smoothing (SES), second exponential smoothing (SEES) and cubic exponential smoothing (CES)(Smyl, 2020). The calculation formula of the SES is as follows:

$$s_t^{(1)} = \alpha y_t + (1-\alpha) s_{t-1}^{(1)} \quad (2)$$

Where s_t^1 is the smooth value of time *t*, y_t represents the actual value of time *t*, and α is the smoothing constant.

The calculation formula of the SEES is as follows:

$$s_t^{(2)} = \alpha s_t^{(1)} + (1-\alpha) s_{t-1}^{(2)} \quad (3)$$

The formula for calculating the predicted value is as follows:

$$\hat{y}_{t+T} = a_t + b_t T \quad (4)$$

Where $\hat{y}_{t+T}$ is the predicted value at $t + T$, t is the current time, T is the predicted time step, a_t is the intercept, b_t is the slope. a_t and b_t are calculated as follows:

$$a_t = 2s_t^{(1)} - s_t^{(2)} \quad (5)$$

$$b_t = \frac{\alpha}{1-\alpha}\left(s_t^{(1)} - s_t^{(2)}\right) \quad (6)$$

The formula of the CES method is calculated as follows:

$$s_t^{(3)} = \alpha s_t^{(2)} + (1-\alpha) s_{t-1}^{(3)} \quad (7)$$

The formula for calculating the predicted value is as follows:

$$\hat{y}_{t+T} = a_t + b_t T + c_t T^2 \quad (8)$$

a_t, b_t, and c_t are calculated as follows:

$$a_t = 3s_t^{(1)} - 3s_t^{(2)} + s_t^{(3)} \quad (9)$$

$$b_t = \frac{\alpha}{2(1-\alpha)^2}\left[(6-5\alpha)s_t^{(1)} - 2(5-4\alpha)s_t^{(2)} + (4-3\alpha)s_t^{(3)}\right] \quad (10)$$

$$c_t = \frac{\alpha^2}{2(1-\alpha)^2}\left(s_t^{(1)} - 2s_t^{(2)} + s_t^{(3)}\right) \quad (11)$$

2.2.3 DNN

Neural network technology originated in the 1950s, when it was called a perceptron, with an input layer, an output layer, and a hidden layer. The input feature vector reaches the output layer through the hidden layer transformation, and the classification result is obtained in the output layer. Deep Neural Networks (DNN) can be understood as a neural network with many hidden layers, also known as deep feedforward network (DFN) and Multi-Layer perceptron (MLP)(Yu et al., 2021). DNN is an emerging algorithm in the field of machine learning in industry and academia in recent years. DNN have significantly improved the simulation capability of the model and have been widely used in many fields.

2.2.4 Markov chain

In nature and social phenomena, some random phenomena follow Markov process, that is, the state of the system or process at t_n can determine the state of the system or process at t_{n+i}. It has nothing to do with the state of the system or process before t_n. For the random process $\{X(t), t \in T\}$, the Markov process expression is as follows:

$$P\{X(t_n) \le x_n | X(t_{n-1}) = x_{n-1}, X(t_{n-2}) = x_{n-2}, \cdots, X(t_1) = x_1\} = P\{X(t_n) \le x_n | X(t_{n-1}) = x_{n-1}\} \tag{12}$$

A Markov chain (MC) is a random process with Markov properties, a special form of Markov process, which is discrete in state and time(Xiang et al., 2021). MC has no aftereffect of Markov process, indicating that its subsequent state is only related to the current state and has nothing to do with the previous state. The expression formula of MC is as follows:

$$P\{X(n+1) = E_{n+1} | X(n) = E_n, X(n-1) = E_{n-1}, \cdots, X(0) = E_0\} = P\{X(n+1) = E_{n+1} | X(n) = E_n\} \tag{13}$$

Here $E = \{E_0, E_1, \cdots, E_n\}$ is the state space set of the random process.

The formula for calculating the *n*-step state transition probability is as follows:

$$P_{ij}^{(n)} = P\{X(m+n) = E_j | X(m) = E_i\} \qquad (E_i, E_j \in E) \tag{14}$$

For all integers $n \ge 0$ and $i, j \in I$, the transition probability $P_{ij}^{(n)}$ of n steps has the following properties:

$$P_{ij}^{(n)} = \sum_{k \in I} P_{ij}^{I} P_{ij}^{(n-1)} \tag{15}$$

$$P_{ij}^{(n)} = \sum_{k_1 \in I} \cdots \sum_{k_{n-1}} P_{ik_1} P_{k_1 k_2} \cdots P_{k_{n-1} j} \tag{16}$$

$$P^{(n)} = P^{(n-1)} P \tag{17}$$

In this study, based on the original Markov chain, the relative error is used as the state process of the Markov chain for state estimation, and the fuzzy set method is used to convert interval predictions into point predictions.

2.2.5 MCMC

The Markov Chain Monte Carlo method (MCMC) was produced in the early 1950s. It is a Monte Carlo method (Monte Carlo) that is simulated by a computer under the framework of Bayesian theory(Reuschen et al., 2020). This method introduces the Markov process into the Monte Carlo simulation, realizes the dynamic simulation in which the sampling distribution changes with the simulation, and makes up for the traditional Monte Carlo integration that can only be statically simulated. MCMC is a simple and effective calculation method, which is widely used in many fields, such as statistics, Bayesian problems, and computer problems.

The logistic regression model was used as a model to study the transition probability of drought and flood in the HRB, and the MCMC method was used to find the optimal parameters of the logistic regression model(Meyers et al., 2021). The logistic regression function is as follows:

$$y(x) = \frac{1}{1+\exp(\alpha+\beta x)} \tag{18}$$

Here α is the position parameter and β is the scale parameter. Under different parameter combinations, the function image is shown in Fig. 2.

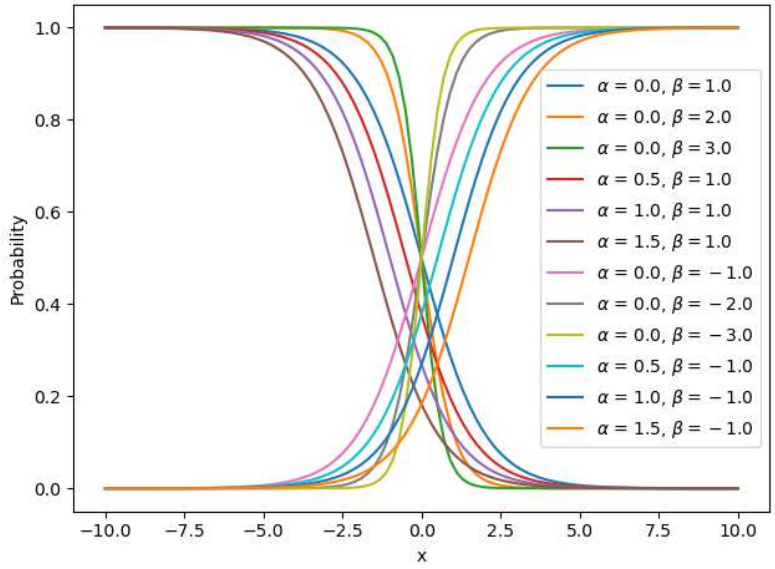

Fig. 2 The shape of the LOGISTIC regression function under different parameter combinations

3 Results

3.1 Runoff sequence analysis

Fig. 3 a1, b1, c1, and d1 depict the change state of runoff sequence of the four hydrological stations respectively. It can be seen from the trend line that the runoff of the four hydrological stations has a downward trend, and the runoff of the HJG station has the fastest decline rate, reaching -6.484 $m^3/s \cdot a^{-1}$. It shows that there is a decreasing trend of water resources in the HRB. Fig.3 a2, a3 are the wavelet power spectra of the runoff at the BH station. It can be seen from the figure that there is a 3-4 year oscillation period in the runoff of the BH station, and the global wavelet spectrum (GWS) exceeds the 95% confidence level. There is also an oscillation period of about 8 years, but it is not significant. Fig.3 b2, b3 are the wavelet power spectra of the runoff of the HLT station. It can be seen from the figure that the runoff at the HLT station has an oscillation period of about 4 years, and the GWS exceeds the 95% confidence level. The other oscillation periods are not significant. Fig.3 c2, c3 are the wavelet power spectra of runoff at HJG station. It can be seen from the figure that the runoff at HJG

station has an oscillation period of about 4 years and about 8 years at the same time, and the GWS exceeds the 95% confidence level. Fig.3 d2, d3 are the wavelet power spectra of HZ station runoff. It can be seen from the figure that there is an obvious oscillation period of about 7-8 years, and the GWS exceeds the 95% confidence level while the other oscillation periods are not significant.

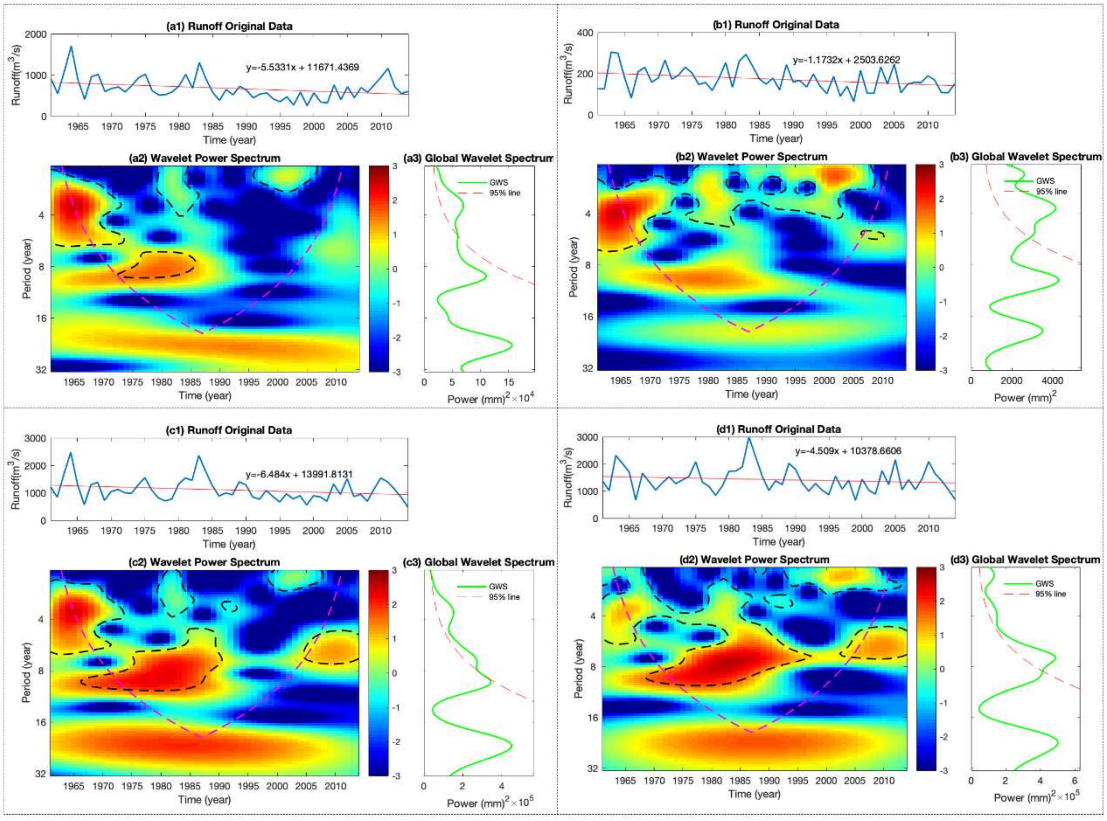

Fig. 3 Wavelet power analysis of runoff from four hydrological stations (a: BH, b: HLT, c: HJG, d: HZ)

STL (Seasonal-Trend decomposition procedure based on Loess) is a common algorithm in time series decomposition. Based on locally weighted scatterplot smoothing (LOESS), the data at a certain time is decomposed into trend component, seasonal component and residual component. Fig.4 a1, a2, a3, and a4 are the STL decomposition results of the BH station runoff. From Fig. 4 a2, it can be seen that the runoff was relatively stable before 1985. After 1985, the runoff began to decrease until the runoff began to rise again in 1998. From Fig. 4 a3, it can be seen that the runoff at the BH station has a cyclical change of about 4 years, and the change trend has been intensified in recent years. From Fig. 4 a4, it can be seen that after removing the trend and periodic changes of the runoff sequence, the residual is relatively stable. Fig.4 b1, b2, b3, and b4 are the STL decomposition results of runoff at HLT station. From Fig. 4 b2, it can be seen that the runoff at the HLT station fluctuated before 1986, and after 1986 the runoff began to decrease continuously. From Fig. 4 b3, it can be seen that the runoff of the HLT station has a cyclic variation of about 3-4 years. From Fig. 4 b4, it can be seen that the residual fluctuations are relatively large, indicating that the runoff sequence of the HLT station has large fluctuations. Fig.4 c1, c2, c3, and c4 are the STL decomposition results of runoff at HJG station. From Fig. 4 c2, it can be seen that the

runoff of HJG station also continued to decrease after 1986, and then the runoff has a slight upward trend after 2000. From Fig. 4 c3, it can be seen that the runoff at HJG station also has a cyclic variation of about 3-4 years. From Fig. 4 c4, it can be seen that after removing the trend and periodic changes of the runoff sequence, the residual fluctuation is small. Fig.4 d1, d2, d3, and d4 are the STL decomposition results of HZ station runoff. From Fig. 4 d2, it can be seen that the runoff at the HZ station has continued to decrease after 1990. From Fig. 4 d3, it can be seen that the runoff at the HZ station also has a cyclic variation of about 3-4 years. From Fig.4 d4, it can be seen that after removing the trend and periodic changes of the runoff sequence, the residual fluctuations are relatively large, indicating that the HZ station runoff has large fluctuations.

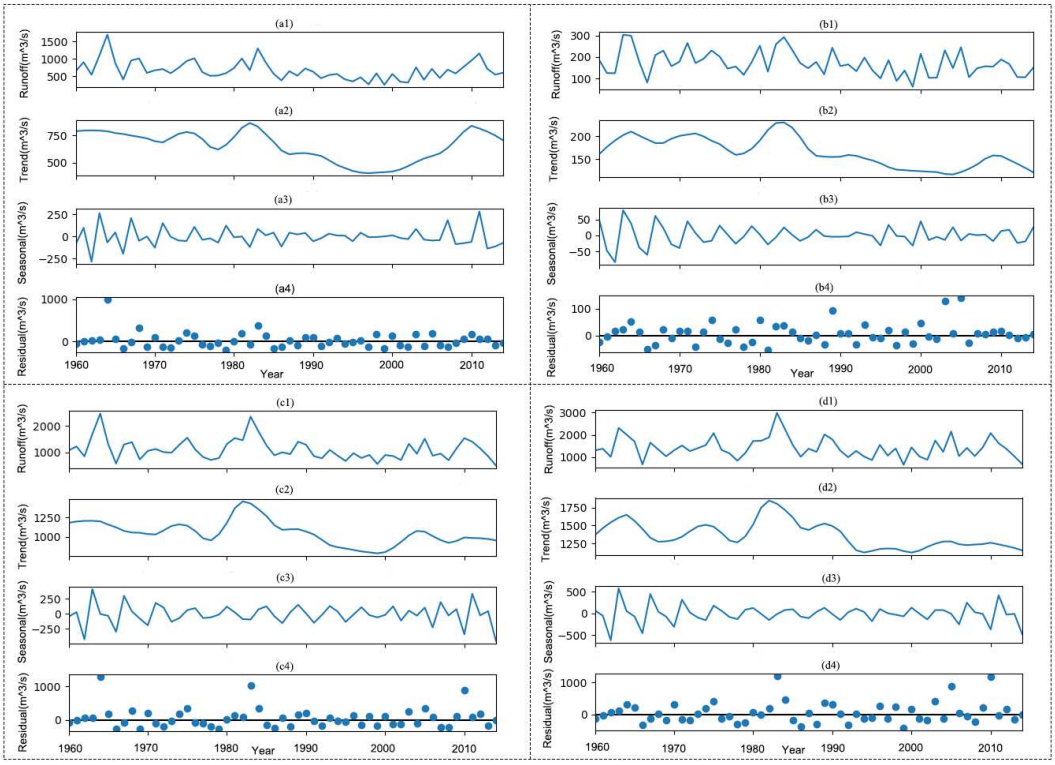

Fig. 4 STL decomposition of runoff from four hydrological stations (a: BH, b: HLT, c: HJG, d: HZ)

3.2 Runoff forecasting

3.2.1 Forecast based on runoff continuity

The SES, SEES, CES, ARIMA, SARIMA, and DNN methods were used to predict runoff by fitting and extending the original sequence reasonably. The period of 1960-2011 was taken as the calibration period, and 2012-2013 as the validation period. Autocorrelation function and partial autocorrelation function graphs are often used in time series analysis and forecasting. They describe the strength of the relationship

between a time series observation and its previous observations. The parameters p and q in AR(p) and MA(q) models are determined by PACF and ACF respectively. Fig. 5 a1 and a2 are the ACF and PACF of the BH station runoff, respectively. From the figure, it can be seen that the runoff has a high correlation with the runoff of the previous step, the correlation exceeding the significance level of 95%, so p is taken as 1, q as 1. Fig. 5 b1 and b2 are the ACF and PACF of HLT station runoff, respectively. It can be seen from the figure that the runoff has little correlation with the previous runoff, and the correlation does not exceed the 95% significance level, so p is taken as 0 , Q as 0. Fig. 5 c1 and c2 are the ACF and PACF of HJG station runoff, respectively. From the figure, it can be seen that the runoff and the previous runoff have the largest correlation within one time step, and the correlation exceeds the 95% significance level, so p is taken as 1, q as 1. Fig. 5 d1 and d2 are the ACF and PACF of HZ station runoff, respectively. It can be seen from the figure that the runoff has little correlation with the previous runoff, and the correlation is less than the significance level of 95%, so p is taken as 0, q as 0.

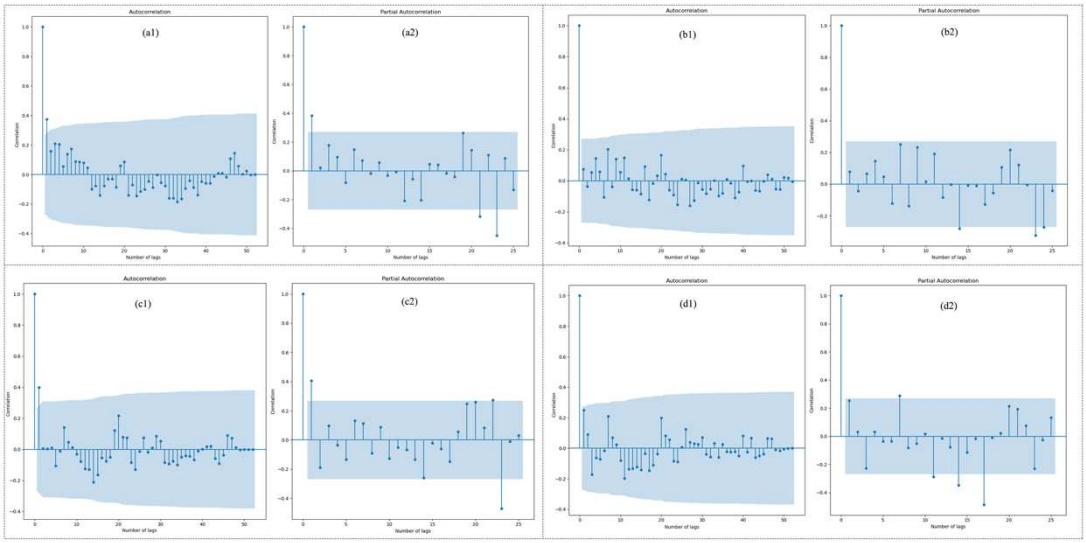

Fig. 5 ACF and PACF diagrams of runoff from the four hydrological stations (a: BH, b: HLT, c: HJG, d: HZ)

Fig. 6 illustrates the runoff simulation results in calibration period (1960-2011) of BH, HLT, HJG, and HZ hydrological stations using SES, SEES, CES, ARIMA, SARIMA, and DNN methods. Seen from left to right, Fig. 6 a1 to Fig. 6 d3 are the simulation results of runoff at four hydrological stations by SES, SEES, and CES respectively. It can be seen from the figure that SES has a better effect on runoff simulation, while SEES and CES are too flat for runoff process simulation and are not sensitive enough to capture runoff changes. Fig. 6 a4 to Fig. 6 d5 are the simulation results of runoff at four hydrological stations by ARIMA and SARIMA methods. It can be seen from the figure that ARIMA and SARIMA can better simulate the change of runoff, and SARIMA can better simulate the change of runoff peak value than ARIMA. Fig. 6 a6 to Fig. 6 d6 are the simulation results of runoff at four hydrological stations by DNN method. It can be seen from the figure that the DNN method can basically simulate the runoff change process. However, the simulation value for some larger runoff processes is too small. The runoff simulation results of the four hydrological

stations from 2012 to 2014 during the validation period are listed in Table 2, which is convenient for comparison with the simulation results based on the Markov chain method.

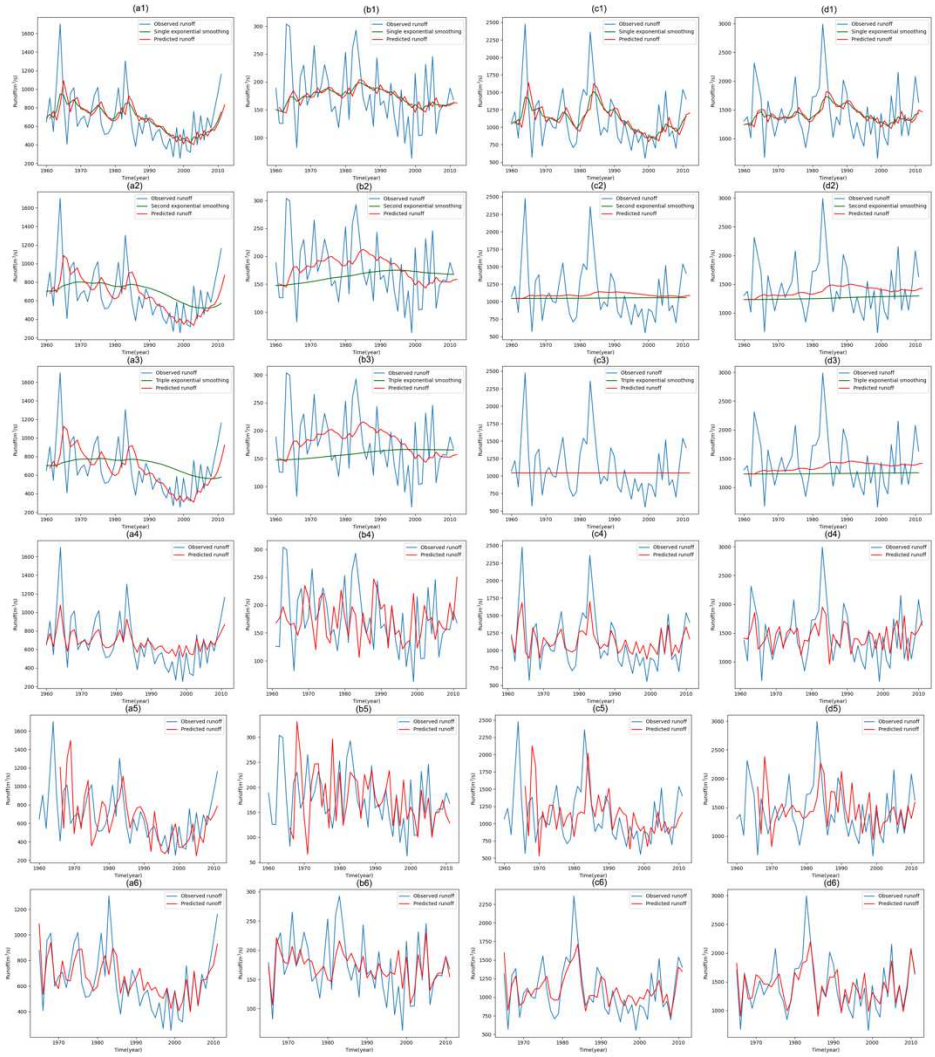

Fig. 6 SES, SEES, CES, ARIMA, SARIMA, and DNN simulation results of runoff at the four hydrological stations in calibration period (a: BH, b: HLT, c: HJG, d: HZ)

3.2.2 Runoff forecast based on Markov chain

Table 1 is the classification result of runoff grades of four hydrological stations using the mean-value mean squared error classification method. The runoff increases from grade 1 to grade 5. Grade 3 roughly represents the state of a flat water year, grade 1 roughly represents the state of a dry year, and grade 5 roughly represents the state of a wet year. Fig. 7 illustrates the result that the runoff of four hydrological stations reaches a stable state through the probability transition matrix in five initial states with the initial probability of 0.2. Fig. 7 a1 to Fig. 7 a5 illustrate the probability of the BH station runoff reaching a stable state in the five states. It can be seen from the figure that the probability of the BH station runoff in state 1 is about 0.13, the probability in state 2 is

about 0.11, the probability in state 3 is about 0.41, the probability in state 4 is about 0.26, and the probability in state 5 is about 0.09. Fig. 7 b1 to Fig. 7 b5 illustrate the probability that the runoff of the HLT station reaches a stable state in the five states. It can be seen from the figure that the probability of HLT station runoff in state 1 is about 0.11, the probability in state 2 is about 0.14, the probability in state 3 is about 0.42, the probability in state 4 is about 0.29, and the probability in state 5 is about 0.04. Fig. 7 c1 to Fig. 7 c5 illustrate the probability when the runoff of the HJG station reaches a stable state in five states. From the figure, it can be seen that the probability of HJG station runoff in state 1 is about 0.13, the probability in state 2 is about 0.11, the probability in state 3 is about 0.40, the probability in state 4 is about 0.23, and the probability in state 5 is about 0.12. Fig. 7 d1 to Fig. 7 d5 illustrate the probability that the runoff of the HZ station reaches a stable state in the five states. It can be seen from the figure that the probability of HZ station runoff in state 1 is about 0.12, the probability in state 2 is about 0.15, the probability in state 3 is about 0.40, the probability in state 4 is about 0.23, and the probability in state 5 is about 0.10.

Table 1 Runoff grouping results based on mean-value mean squared error method (m^3/s)

ST	Class				
	1	2	3	4	5
BH	<378.3	[378.3, 542.1)	[542.1, 815.1)	[815.1, 979.0)	979.0≤
HLT	<109.8	[109.8, 144.2)	[144.2, 201.5)	[201.5, 235.9)	235.9≤
HJG	<688.2	[688.2, 923.5)	[923.5, 1315.7)	[1315.7, 1551.0)	1551.0≤
HZ	<935.0	[935.0, 1206.6)	[1206.6, 1659.3)	[1659.3, 1930.9)	1930.9≤

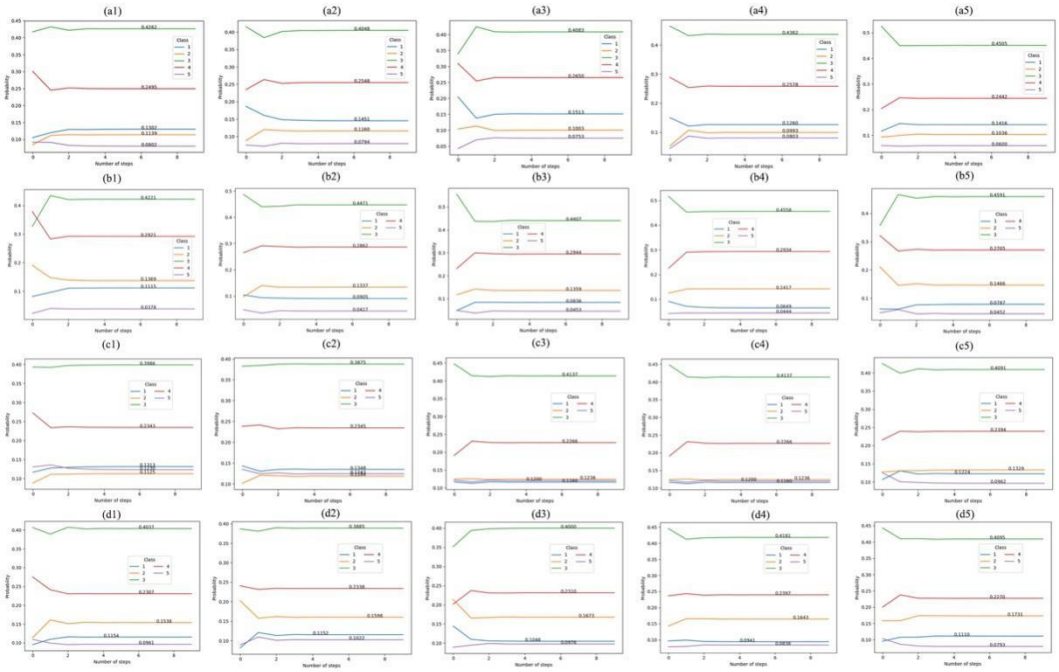

Fig. 7 Probability of the five states of runoff from four hydrological stations reaching the stable stage under 1 to 5 steps (a: BH, b: HLT, c: HJG, d: HZ)

Based on the original runoff Markov forecasting model (MFM), the relative error between the original runoff and the fitted runoff was used as the original data of the

MFM, so that the hidden information in the original runoff data can be used to a greater extent. Fig. 8 illustrates the process of fitting the original runoff with different fitting methods, including moving average method, mean value method, linear spline curve, quadric spline curve, and cubic spline curve. This constitutes a moving average Markov forecasting model (MA-MFM), a mean Markov forecasting model (M-MFM), a linear spline Markov forecasting model (LS-MFM), a quadric spline Markov forecasting model (QS-MFM), and a cubic spline Markov forecasting model (CS-MFM).

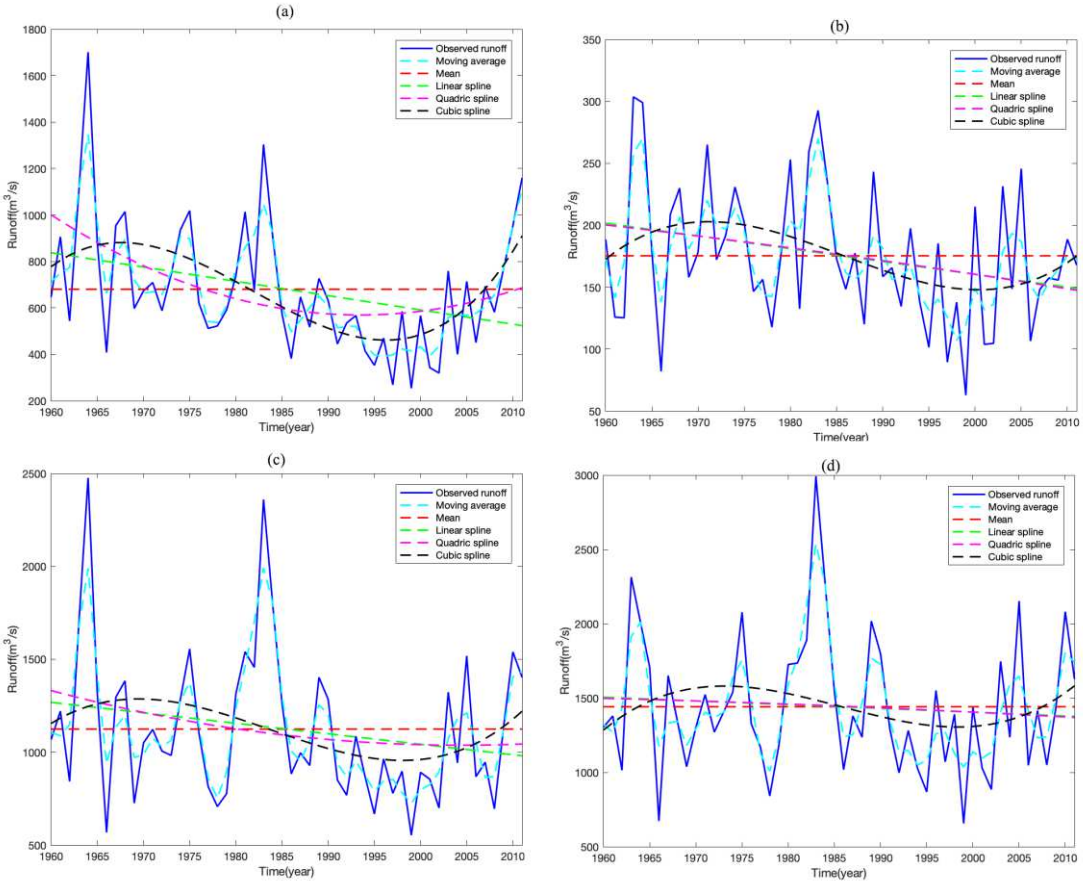

Fig. 8 Simulation of runoff process in four hydrological stations with different fitting methods (a: BH, b: HLT, c: HJG, d: HZ)

Table 2 lists the observed runoff (OR) and simulated runoff results of all methods during the validation period. Table 3 lists the relative error results between the simulated runoff and the measured runoff. Fig. 9 is the cumulative histogram of the cumulative absolute error of all methods during the validation period. Combining the three, it can be seen that the more stable the runoff change, the more favorable it is for the prediction. For example, the 2012-2013 runoff change at the BH station is relatively stable. MFM, M-MFM, and QS-MFM all have good prediction results, and the cumulative absolute error is less than 0.5. However, the runoff of HJG station and HZ station in 2014 has a significant decrease compared with the runoff in 2013, which is such a drastic change as most methods cannot predict. On the whole, QS-MFM, MFM, MA-MFM, CES, and DNN have strong generalization ability for runoff prediction, and can adapt to the simulation of drastic changes in runoff. However, the simulation capabilities of ARIMA and SARIME forecasting methods are not stable. For example,

ARIMA has good results for BH station runoff simulation, but has poor performance for HLT station runoff simulation. SARIMA has a poor effect on BH station runoff simulation, but has a good result in HLT station runoff simulation. The CS-MFM has the worst simulation effect, and the runoff simulation ability of the four stations is relatively poor.

Table 2 Runoff simulation results of four hydrological stations during the validation period with different prediction methods

ST	Year	OR	MFM	MA-MFM	M-MFM	LS-MFM	QS-MFM	CS-MFM	SES	SEES	CES	ARIMA	SARIMA	DNN
BH	2012	715.7	710.5	1009.2	685.6	455.4	660.4	986.8	831.4	874.5	925.2	869.4	828.4	966.4
	2013	548.8	647.7	759.8	636.5	557.9	661.8	921.6	734.3	814.5	870.9	756.7	1156.1	707.9
	2014	602.7	603.5	539.7	634.8	549.0	715.0	1033.6	673.4	732.1	755.7	713.2	993.3	529.7
HLT	2012	107.5	175.5	162.5	167.5	172.0	170.1	166.2	161.9	158.4	156.8	250.4	142.5	150.0
	2013	106.4	173.6	125.2	165.0	180.2	121.1	159.3	152.1	152.0	150.3	154.1	144.3	155.4
	2014	150.8	162.9	105.1	148.4	220.3	139.8	151.4	146.3	146.1	144.2	155.6	181.0	147.9
HJG	2012	1145.7	1025.5	1327.8	1183.4	918.5	1008.5	1473.1	1202.5	1087.5	1043.9	1163.7	945.6	1335.7
	2013	847.0	861.5	1180.7	1069.2	926.5	996.3	1065.8	1144.8	1088.9	1043.9	1124.1	1029.8	1149.6
	2014	489.7	1026.7	871.4	1081.4	900.5	971.5	1436.8	1042.6	1084.2	1043.9	1123.2	1086.8	865.6
HZ	2012	1368.2	1359.4	1605.2	1359.4	1287.0	1279.5	1824.5	1465.8	1427.7	1418.8	1488.0	1424.2	1622.0
	2013	1035.1	1370.3	1346.3	1271.3	1908.7	1689.9	1340.3	1422.5	1426.6	1418.7	1453.5	1242.0	1315.6
	2014	682.3	1443.3	1057.7	1349.8	1165.1	1204.5	1401.8	1347.3	1412.2	1408.7	1444.9	1587.7	1326.6

Table 3 The relative error results of the runoff simulation of the four hydrological stations during the validation period with different prediction methods

ST	Year	MFM	MA-MFM	M-MFM	LS-MFM	QS-MFM	CS-MFM	SES	SEES	CES	ARIMA	SARIMA	DNN
BH	2012	-0.01	0.41	-0.04	-0.36	-0.08	0.38	0.16	0.22	0.29	0.21	0.16	0.35
	2013	0.18	0.38	0.16	0.02	0.21	0.68	0.34	0.48	0.59	0.38	1.11	0.29
	2014	0.00	-0.10	0.05	-0.09	0.19	0.71	0.12	0.21	0.25	0.18	0.65	-0.12
HLT	2012	0.63	0.51	0.56	0.60	0.58	0.55	0.51	0.47	0.46	1.33	0.33	0.40
	2013	0.63	0.18	0.55	0.69	0.14	0.50	0.43	0.43	0.41	0.45	0.36	0.46
	2014	0.08	-0.30	-0.02	0.46	-0.07	0.00	-0.03	-0.03	-0.04	0.03	0.20	-0.02
HJG	2012	-0.10	0.16	0.03	-0.20	-0.12	0.29	0.05	-0.05	-0.09	0.02	-0.17	0.17
	2013	0.02	0.39	0.26	0.09	0.18	0.26	0.35	0.29	0.23	0.33	0.22	0.36
	2014	1.10	0.78	1.21	0.84	0.98	1.93	1.13	1.21	1.13	1.29	1.22	0.77
HZ	2012	-0.01	0.17	-0.01	-0.06	-0.06	0.33	0.07	0.04	0.04	0.09	0.04	0.19
	2013	0.32	0.30	0.23	0.84	0.63	0.29	0.37	0.38	0.37	0.40	0.20	0.27
	2014	1.12	0.55	0.98	0.71	0.77	1.05	0.97	1.07	1.06	1.12	1.33	0.94

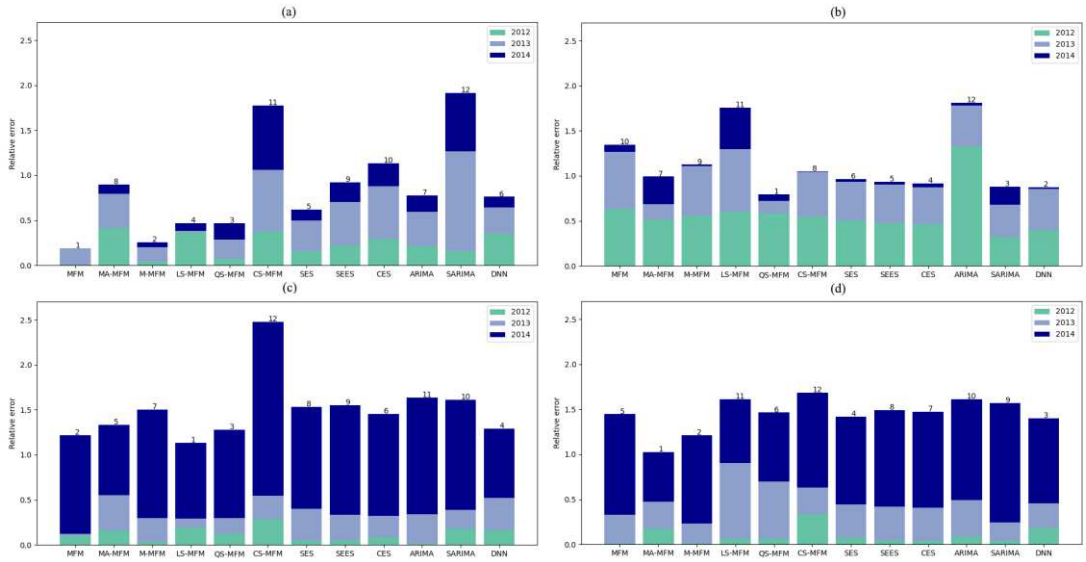

Fig. 9 The cumulative relative error results of the runoff simulation of the four hydrological stations during the validation period with different prediction methods (a: BH, b: HLT, c: HJG, d: HZ)

3.2.3 Dry and wet conversion analysis

Fig. 10 shows the fitting results of P-III curve of runoff from four hydrological stations. Generally, the 25% score is used as the demarcation point for wet years and the 75% score is used as the demarcation point for dry years. The P-III curve was used to extract the high and low runoff boundary points of the four hydrological stations, and then the runoff time series were classified. The runoff with a score greater than 25% is classified as a wet year, and the runoff with a score less than 75% is classified as a dry year.

Fig. 11 is the result of using the MCMC method to optimize the parameters of the Logistic model, and then fitting the wet and dry conditions. Among them, the probability density of parameter distribution is the largest, and the point is selected as the optimal parameter. For example, the α parameter of the Logistics model of BH station is 16.7562, and the β parameter is -0.0273. The Logistic model with MCMC optimized parameters can simulate the high and low runoff changes well, and it is basically a smooth transition curve from the low-runoff state to the high-runoff state.

Table 4 lists the transition probability of runoff from low to high (high to low). It can be seen from the table that the probability of a wet year is 0.29% when the runoff at the BH station at 400 m^3/s, and the probability of a dry year is 99.71%. It can be concluded that the flow of 400 m^3/s is a dry year at the BH station. The probability of a wet year is 40.61% with the flow of 600 m^3/s, and the probability of a dry year is 59.39%, indicating that the flow of 600 m^3/s basically belongs to the state of a normal water year at the BH station. The probability of a wet year with a flow of 900 m^3/s is 99.96%, and the probability of a dry year is 0.04%. It can be said that the flow of 900m^3/s at the BH station has a high probability of being in a wet year. In the same way, the probability that the runoff from HLT, HJG, and HZ stations is low to high (high to low) can be

obtained. Among them, the HLT station has the fastest conversion rate of drought and flood, and the flow that generates floods is 6 times that of drought. It shows that the smaller the catchment area, the faster the conversion rate of drought to flood, while the larger the catchment area, the more stable the conversion of drought to flood.

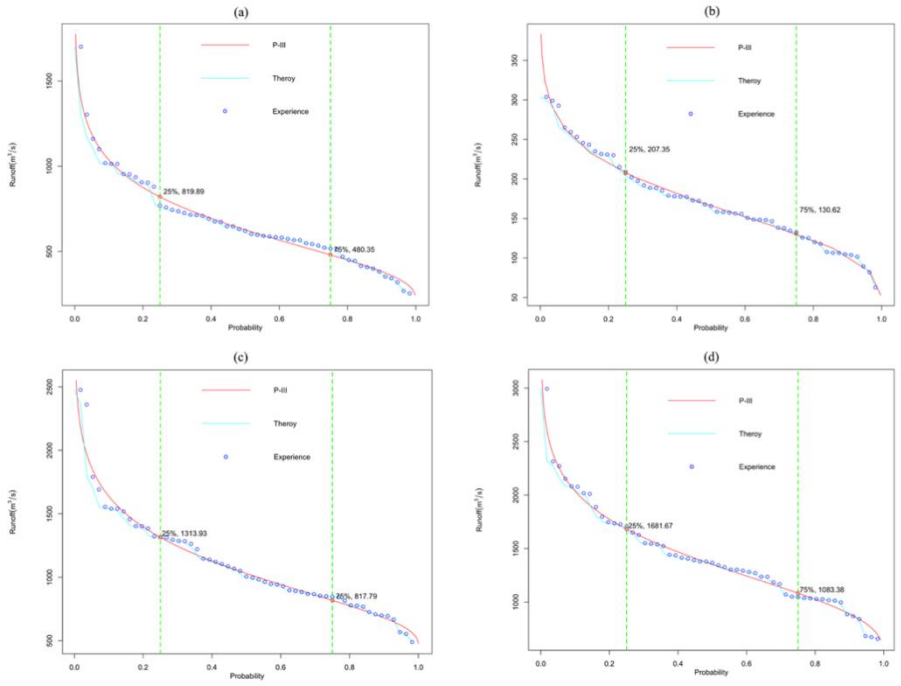

Fig. 10 Runoff P-III curve fitting of four hydrological stations (a: BH, b: HLT, c: HJG, d: HZ)

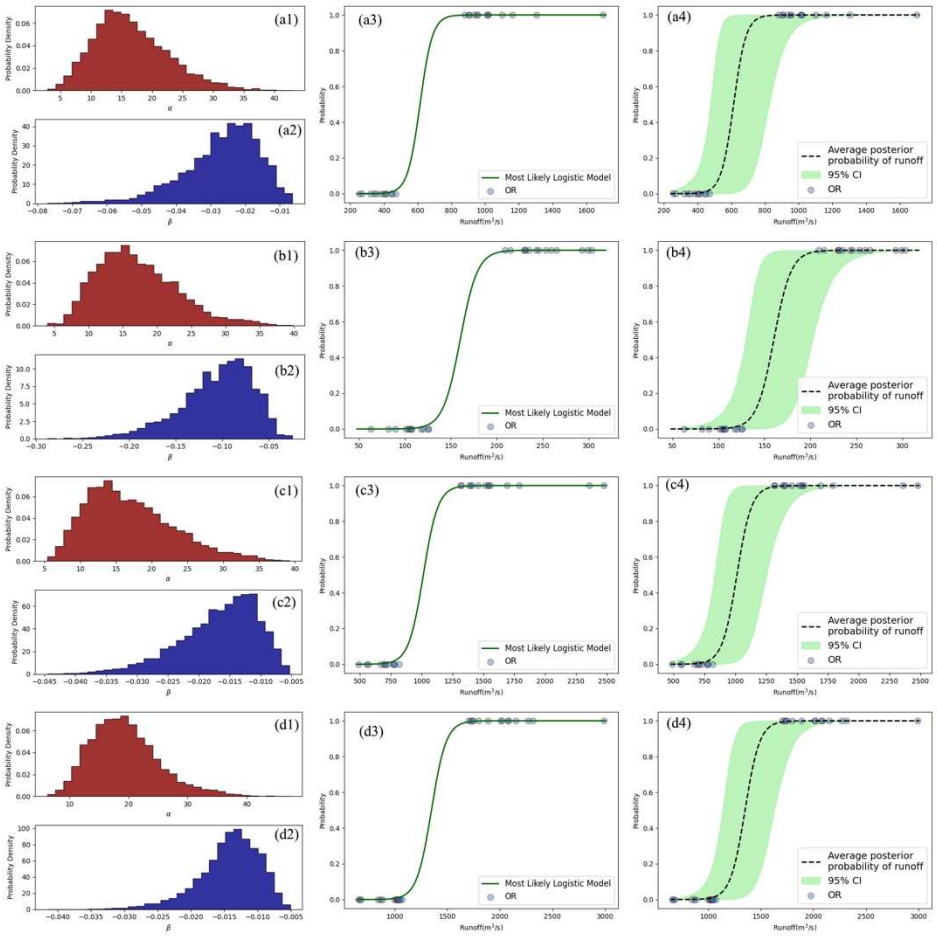

Fig. 11 Logistic model parameter selection, model fitting and posterior probability distribution fitting of the four hydrological runoff (a: BH, b: HLT, c: HJG, d: HZ)

Table 4 Low to high (high to low) conversion probability of runoff at four hydrological stations

ST	Runoff(m^3/s)-probability(100%)					
	400	500	600	700	800	900
BH	0.29% (99.71%)	4.27% (95.73%)	40.61% (59.39%)	91.29% (8.71%)	99.38% (0.62%)	99.96% (0.04%)
	50	100	150	200	250	300
HLT	0.00% (100.00%)	0.16% (99.84%)	24.98% (75.02%)	98.56% (1.44%)	99.99% (0.01%)	100.00% (0.00%)
	800	900	1000	1100	1200	1300
HJG	2.70% (97.30%)	12.98% (87.02%)	44.47% (55.53%)	81.13% (18.87%)	95.85% (4.15%)	99.20% (0.80%)
	800	1000	1200	1400	1600	1800
HZ	0.04% (99.96%)	0.65% (99.35%)	10.36% (89.64%)	66.99% (33.01%)	97.27% (2.73%)	99.84% (0.16%)

4 Discussion

It is worth noting that whether it is based on the change trend of the runoff sequence or the runoff prediction based on the Markov chain, all information needs to be obtained from the original data(Qu et al., 2020; Yu et al., 2020). If the data has a certain regular change, such as a linear trend change, this will make prediction an easy task. However, if there is a sudden change in the data, it will change the trend of the original sequence, making prediction a difficult task(Feng et al., 2011). Fig. 12 illustrates the results of the runoff mutation test of four hydrological stations. It can be seen from the figure that there are mutation points in the runoff of the four hydrological stations, especially in HLT, HJG, and HZ stations, which makes the prediction of runoff in different periods of time different. The method can be tried is to do mutation detection on the time series first, and then only use the data after the mutation. However, this will reduce the data that can be used, and will make the data lack representativeness(Chen et al., 2020).

Of course, the prediction of runoff can also be based on the teleconnection prediction of the climate background. However, this method needs to find the factors that have the greatest impact on runoff changes, which increases the difficulty of the operability of the prediction(Wang et al., 2015; Xie et al., 2019). Meanwhile, the runoff prediction based on teleconnection will be more towards the real physical basis, which will make the runoff prediction results have a physical basis(Badrzadeh et al., 2015). In future research, a runoff prediction method based on teleconnection and weather background can be developed in the HRB.

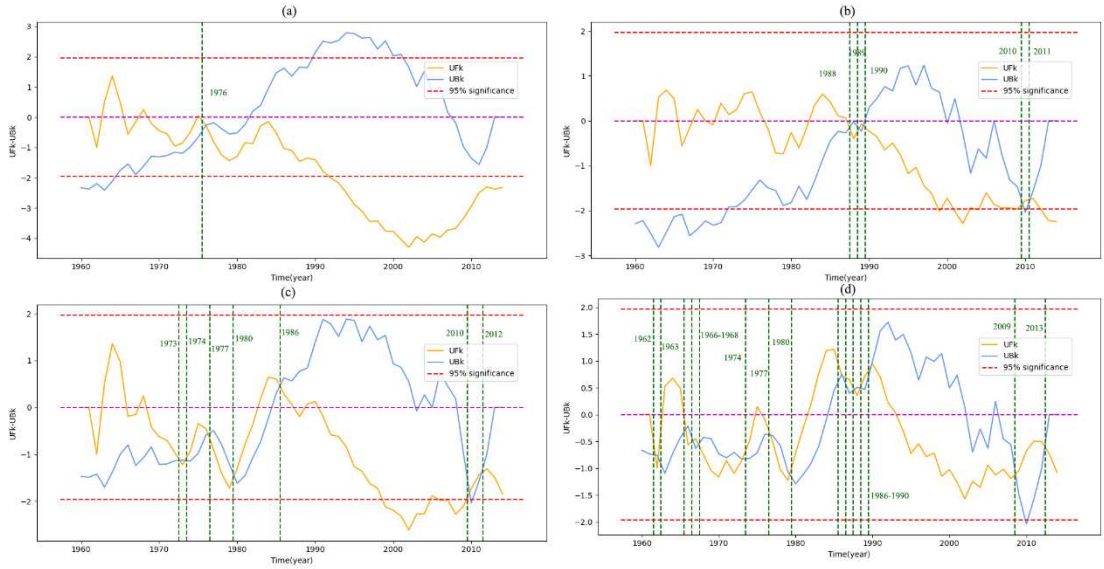

Fig. 12 MK trend and mutation test of runoff from four hydrological stations (a: BH, b: HLT, c: HJG, d: HZ)

5 Conclusions

In this study, the historical runoff information of four hydrological stations in the HRB was used to simulate and predict runoff by using 12 methods. Then the MCMC

method was used to analyze the low-high (high-low) transition probability of annual runoff in the HRB. The following main conclusions can be drawn from this study:

(1) The runoff processes recorded by the four hydrological stations in the HRB all show different degrees of decline. Among them, the runoff at the HJG station has the fastest decline rate, reaching -6.484 $m3/s \cdot a^{-1}$. The runoff of the four hydrological stations has an oscillating period of about 3-4 years, and the runoff showed an obvious downward trend in the mid-1980s.

(2) The smoother the runoff changes, the higher the probability of accurate prediction. Among the 12 methods, QS-MFM, MFM, MA-MFM, CES and DNN all have strong generalization capabilities and can predict runoff changes more accurately. The prediction ability of ARIMA and SRIMA methods is unstable, and the prediction ability of CS-MFM is the worst.

(3) The MCMC method can accurately estimate the parameters of the Logistic model, and the high and low runoff transition probability model constructed in the HRB can accurately calculate the low-high (high-low) runoff transition probability.

Although the prediction method used in this study can predict the runoff of the HRB accurately, it is based on statistical methods. In the runoff sequence of the HRB, however, there is a sudden change, which will affect the accuracy and continuity of the prediction. Therefore, prediction methods based on teleconnection and weather systems are worthy of discussion in future research.

Acknowledgments The research is financially supported by National Natural Science Foundation of China (Grant No. U1911204， 51861125203), National Key R&D Program of China (2017YFC0405900), The Project for Creative Research from Guangdong Water Resources Department (Grant No. 2018, 2020).

Competing Interests The authors declare no conflict of interest.

References

Archer, D.R., Fowler, H.J., 2008. Using meteorological data to forecast seasonal runoff on the River Jhelum, Pakistan. J. Hydrol. 361, 10–23. https://doi.org/https://doi.org/10.1016/j.jhydrol.2008.07.017

Badrzadeh, H., Sarukkalige, R., Jayawardena, A.W., 2015. Hourly runoff forecasting for flood risk management: Application of various computational intelligence models. J. Hydrol. 529, 1633–1643. https://doi.org/https://doi.org/10.1016/j.jhydrol.2015.07.057

Carmona-Benítez, R.B., Nieto, M.R., 2020. SARIMA damp trend grey forecasting model for airline industry. J. Air Transp. Manag. 82, 101736. https://doi.org/https://doi.org/10.1016/j.jairtraman.2019.101736

Chen, X., Huang, J., Han, Z., Gao, H., Liu, M., Li, Z., Liu, X., Li, Q., Qi, H., Huang, Y., 2020. The importance of short lag-time in the runoff forecasting model based on long short-term memory. J. Hydrol. 589, 125359. https://doi.org/https://doi.org/10.1016/j.jhydrol.2020.125359

Cheng, B., Li, H., Yue, S., Huang, K., 2019. A conceptual decision-making for the ecological base flow of rivers considering the economic value of ecosystem services of rivers in water shortage area of Northwest China. J. Hydrol. 578, 124126. https://doi.org/https://doi.org/10.1016/j.jhydrol.2019.124126

Chua, L.H.C., Wong, T.S.W., 2011. Runoff forecasting for an asphalt plane by Artificial Neural Networks and comparisons with kinematic wave and autoregressive moving average models. J. Hydrol. 397, 191–201. https://doi.org/https://doi.org/10.1016/j.jhydrol.2010.11.030

Deng, C., Zhang, G., Li, Z., Li, K., 2020. Interprovincial food trade and water resources conservation in China. Sci. Total Environ. 737, 139651. https://doi.org/https://doi.org/10.1016/j.scitotenv.2020.139651

Dong, H., Feng, Z., Yang, Y., Li, P., You, Z., 2021. Sustainability assessment of critical natural capital: a case study of water resources in Qinghai Province, China. J. Clean. Prod. 286, 125532. https://doi.org/https://doi.org/10.1016/j.jclepro.2020.125532

Doycheva, K., Horn, G., Koch, C., Schumann, A., König, M., 2017. Assessment and weighting of meteorological ensemble forecast members based on supervised machine learning with application to runoff simulations and flood warning. Adv. Eng. Informatics 33, 427–439. https://doi.org/https://doi.org/10.1016/j.aei.2016.11.001

Feng, J., Li, L., Yang, N., Hong, Y., Pang, M., Yao, X., Wang, L., 2011. Critical chain construction with multi-resource constraints based on portfolio technology in South-to-North Water Diversion Project. Water Sci. Eng. 4, 225–236. https://doi.org/https://doi.org/10.3882/j.issn.1674-2370.2011.02.010

Ferrucci, A., Vocciante, M., 2021. Improved management of water resources in process industry by accounting for fluctuations of water content in feed streams and products. J. Water Process Eng. 39, 101870. https://doi.org/https://doi.org/10.1016/j.jwpe.2020.101870

Ghumman, A.R., Ghazaw, Y.M., Sohail, A.R., Watanabe, K., 2011. Runoff forecasting by artificial neural network and conventional model. Alexandria Eng. J. 50, 345–350. https://doi.org/https://doi.org/10.1016/j.aej.2012.01.005

Guo, C., Chen, Y., Xia, W., Qu, X., Yuan, H., Xie, S., Lin, L.-S., 2020. Eutrophication and heavy metal pollution patterns in the water suppling lakes of China's south-to-north water diversion project. Sci. Total Environ. 711, 134543. https://doi.org/https://doi.org/10.1016/j.scitotenv.2019.134543

He, X., Luo, J., Li, P., Zuo, G., Xie, J., 2020. A Hybrid Model Based on Variational Mode Decomposition and Gradient Boosting Regression Tree for Monthly Runoff Forecasting. Water Resour. Manag. 34, 865–884. https://doi.org/10.1007/s11269-020-02483-x

Khan, M.M.H., Muhammad, N.S., El-Shafie, A., 2020. Wavelet based hybrid ANN-ARIMA models for meteorological drought forecasting. J. Hydrol. 590, 125380. https://doi.org/https://doi.org/10.1016/j.jhydrol.2020.125380

Li, B., Biswas, A., Wang, Y., Li, Z., 2021. Identifying the dominant effects of climate and land use change on soil water balance in deep loessial vadose zone. Agric. Water Manag. 245, 106637. https://doi.org/https://doi.org/10.1016/j.agwat.2020.106637

Li, J., Liu, Z., He, C., Yue, H., Gou, S., 2017. Water shortages raised a legitimate concern over the sustainable development of the drylands of northern China: Evidence from the water stress index. Sci. Total Environ. 590–591, 739–750. https://doi.org/https://doi.org/10.1016/j.scitotenv.2017.03.037

Liu, Q., 2014. An Improved SA-Based BP-ANN Technique for Annual Runoff Forecasting Under Uncertain Environment BT - Proceedings of the Seventh International Conference on Management Science and Engineering Management, in: Xu, J., Fry, J.A., Lev, B., Hajiyev, A. (Eds.), . Springer Berlin Heidelberg, Berlin, Heidelberg, pp. 1467–1474.

Löwe, R., Mikkelsen, P.S., Madsen, H., 2014. Stochastic rainfall-runoff forecasting: parameter estimation, multi-step prediction, and evaluation of overflow risk. Stoch. Environ. Res. Risk Assess. 28, 505–516. https://doi.org/10.1007/s00477-013-0768-0

Ma, X.X., Zhu, H.Q., Xiao, Y., Wang, W.S., Wang, H.L., Zhang, J.W., 2020. Inspection method for random simulation of runoff sequence based on sample entropy and statistical parameters. J. Hydrol. 581, 124392. https://doi.org/https://doi.org/10.1016/j.jhydrol.2019.124392

Meyers, S.D., Landry, S., Beck, M.W., Luther, M.E., 2021. Using logistic regression to model the risk of sewer overflows triggered by compound flooding with application to sea level rise. Urban Clim. 35, 100752. https://doi.org/https://doi.org/10.1016/j.uclim.2020.100752

Moosavi, V., Talebi, A., Hadian, M.R., 2017. Development of a Hybrid Wavelet Packet- Group Method of Data Handling (WPGMDH) Model for Runoff Forecasting. Water Resour. Manag. 31, 43–59. https://doi.org/10.1007/s11269-016-1507-3

Nygren, M., Giese, M., Kløve, B., Haaf, E., Rossi, P.M., Barthel, R., 2020. Changes in seasonality of groundwater level fluctuations in a temperate-cold climate transition zone. J. Hydrol. X 8, 100062. https://doi.org/https://doi.org/10.1016/j.hydroa.2020.100062

Ouyang, R., Cheng, W., Wang, W., Jiang, Y., Zhang, Y., Wang, Y., 2007. Research on runoff forecast approaches to the Aksu River basin. Sci. China Ser. D Earth Sci. 50, 16–25. https://doi.org/10.1007/s11430-007-5008-3

Pan, T., Wang, R., 2004. State space neural networks for short term rainfall-runoff forecasting. J. Hydrol. 297, 34–50. https://doi.org/https://doi.org/10.1016/j.jhydrol.2004.04.010

Parida, B.P., Moalafhi, D.B., Kenabatho, P.K., 2006. Forecasting runoff coefficients using ANN for water resources management: The case of Notwane catchment in Eastern Botswana. Phys. Chem. Earth, Parts A/B/C 31, 928–934. https://doi.org/https://doi.org/10.1016/j.pce.2006.08.017

Piotrowski, A.P., Napiorkowski, J.J., 2012. Product-Units neural networks for catchment runoff forecasting. Adv. Water Resour. 49, 97–113. https://doi.org/https://doi.org/10.1016/j.advwatres.2012.05.016

Qi, B., Liu, H., Zhao, S., Liu, B., 2020. Observed precipitation pattern changes and potential runoff generation capacity from 1961–2016 in the upper reaches of the Hanjiang River Basin, China. Atmos. Res. 105392. https://doi.org/https://doi.org/10.1016/j.atmosres.2020.105392

Qu, X., Chen, Y., Liu, H., Xia, W., Lu, Y., Gang, D.-D., Lin, L.-S., 2020. A holistic assessment of water quality condition and spatiotemporal patterns in impounded lakes along the eastern route of China's South-to-North water diversion project. Water Res. 185, 116275. https://doi.org/https://doi.org/10.1016/j.watres.2020.116275

Reuschen, S., Xu, T., Nowak, W., 2020. Bayesian inversion of hierarchical geostatistical models using a parallel-tempering sequential Gibbs MCMC. Adv. Water Resour. 141, 103614. https://doi.org/https://doi.org/10.1016/j.advwatres.2020.103614

Sedki, A., Ouazar, D., El Mazoudi, E., 2009. Evolving neural network using real coded genetic algorithm for daily rainfall–runoff forecasting. Expert Syst. Appl. 36, 4523–4527. https://doi.org/https://doi.org/10.1016/j.eswa.2008.05.024

Shappell, N.W., Shipitalo, M.J., Billey, L.O., 2021. Estrogenicity of agricultural runoff: A rainfall simulation study of worst-case scenarios using fresh layer and roaster litter, and farrowing swine manure. Sci. Total Environ. 750, 141188. https://doi.org/https://doi.org/10.1016/j.scitotenv.2020.141188

Smyl, S., 2020. A hybrid method of exponential smoothing and recurrent neural networks for time series forecasting. Int. J. Forecast. 36, 75–85. https://doi.org/https://doi.org/10.1016/j.ijforecast.2019.03.017

Tian, W., Liu, X., Liu, C., Bai, P., 2018. Investigation and simulations of changes in the relationship of precipitation-runoff in drought years. J. Hydrol. 565, 95–105. https://doi.org/https://doi.org/10.1016/j.jhydrol.2018.08.015

Turunen, M., Gurarslan, G., Šimůnek, J., Koivusalo, H., 2020. What is the worth of drain discharge and surface runoff data in hydrological simulations? J. Hydrol. 587, 125030. https://doi.org/https://doi.org/10.1016/j.jhydrol.2020.125030

Wang, W., Chau, K., Qiu, L., Chen, Y., 2015. Improving forecasting accuracy of medium and long-term runoff using artificial neural network based on EEMD decomposition. Environ. Res. 139, 46–54. https://doi.org/https://doi.org/10.1016/j.envres.2015.02.002

Wu, J., 2018. Co-evolution Algorithm for Parameter Optimization of RBF Neural Networks for Rainfall-Runoff Forecasting BT - Intelligent Computing Theories and Application, in: Huang, D.-S., Bevilacqua, V., Premaratne, P., Gupta, P. (Eds.), . Springer International Publishing, Cham, pp. 195–206.

Xiang, X., Fu, H., Zhou, J., Deng, Y., Yang, X., 2021. Taboo rate and hitting time distribution of continuous-time reversible Markov chains. Stat. Probab. Lett. 169, 108969. https://doi.org/https://doi.org/10.1016/j.spl.2020.108969

Xie, T., Zhang, G., Hou, J., Xie, J., Lv, M., Liu, F., 2019. Hybrid forecasting model for non-stationary daily runoff series: A case study in the Han River Basin, China. J. Hydrol. 577, 123915. https://doi.org/https://doi.org/10.1016/j.jhydrol.2019.123915

Xiu-fen, Z., Li-shan, K., Hong-qing, C., Zhi-jian, W., 2003. A hybrid model for the mid-long term runoff forecasting by evolutionary computation techniques. Wuhan Univ. J. Nat. Sci. 8, 234–238. https://doi.org/10.1007/BF02899485

Yaduvanshi, A., Nkemelang, T., Bendapudi, R., New, M., 2021. Temperature and rainfall extremes change under current and future global warming levels across Indian climate zones. Weather Clim. Extrem. 31, 100291. https://doi.org/https://doi.org/10.1016/j.wace.2020.100291

Yang, Q., Yu, Z., Wei, J., Yang, C., Gu, H., Xiao, M., Shang, S., Dong, N., Gao, L., Arnault, J., Laux, P., Kunstmann, H., 2021. Performance of the WRF model in simulating intense precipitation events over the Hanjiang River Basin, China – A multi-physics ensemble approach. Atmos. Res. 248, 105206. https://doi.org/https://doi.org/10.1016/j.atmosres.2020.105206

Yu, X., Sreekanth, J., Cui, T., Pickett, T., Xin, P., 2021. Adaptative DNN emulator-enabled multi-objective optimization to manage aquifer–sea flux interactions in a regional coastal aquifer. Agric. Water Manag. 245, 106571. https://doi.org/https://doi.org/10.1016/j.agwat.2020.106571

Yu, Z., Wang, H., Miao, M., Kong, Q., Quan, Q., Wang, R., Liu, J., 2020. Long-term monitoring of community succession in impoundment lake: Responses of macroinvertebrate to South-to-North Water Diversion Project. Ecol. Indic. 118, 106734. https://doi.org/https://doi.org/10.1016/j.ecolind.2020.106734

Zhou, Y., Guo, S., Hong, X., Chang, F.-J., 2017. Systematic impact assessment on inter-basin water transfer projects of the Hanjiang River Basin in China. J. Hydrol. 553, 584–595. https://doi.org/https://doi.org/10.1016/j.jhydrol.2017.08.039

Figures

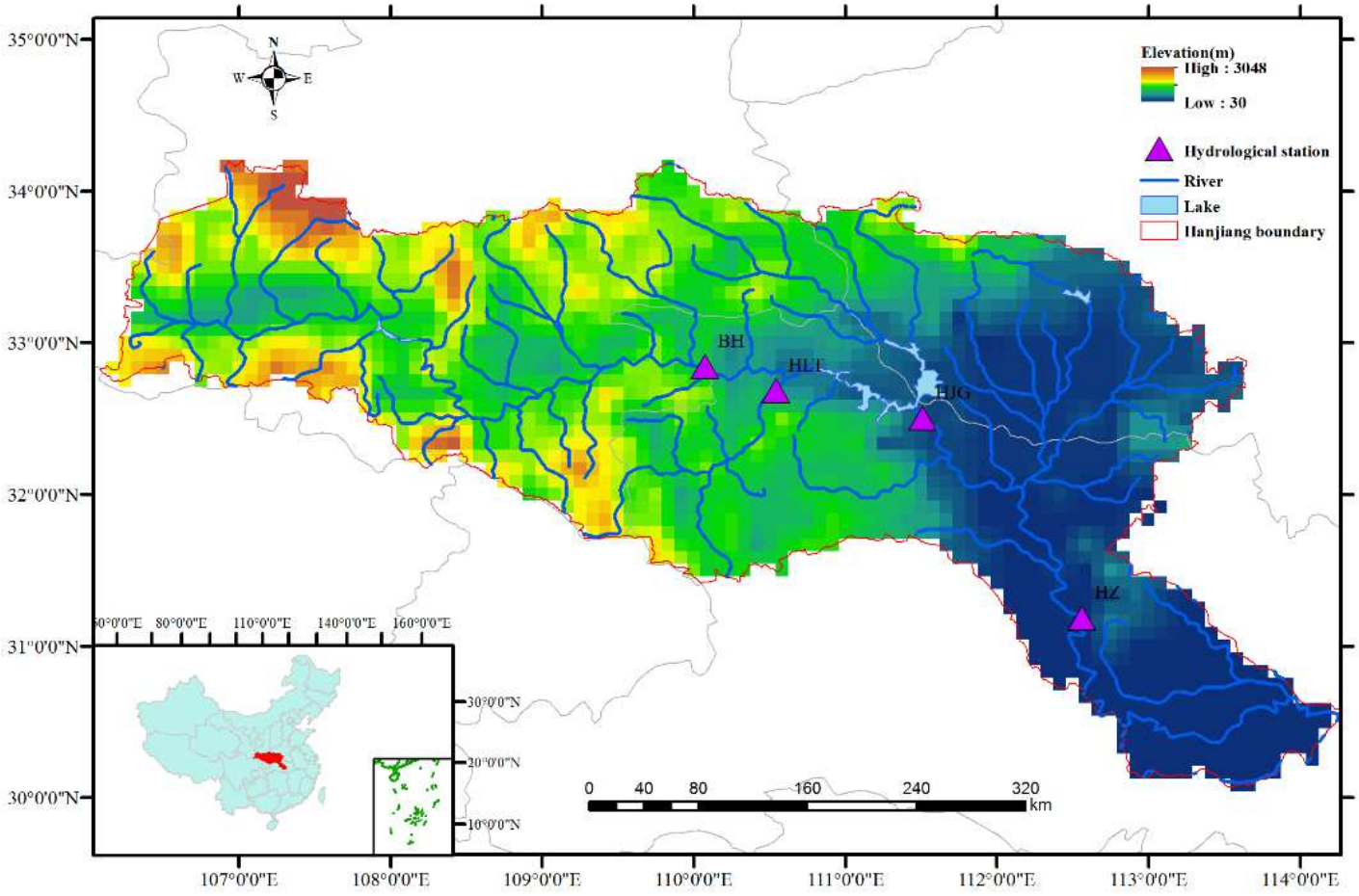

Figure 1

Topography of the study area and distribution of the hydrological stations. Note: The designations employed and the presentation of the material on this map do not imply the expression of any opinion whatsoever on the part of Research Square concerning the legal status of any country, territory, city or area or of its authorities, or concerning the delimitation of its frontiers or boundaries. This map has been provided by the authors.

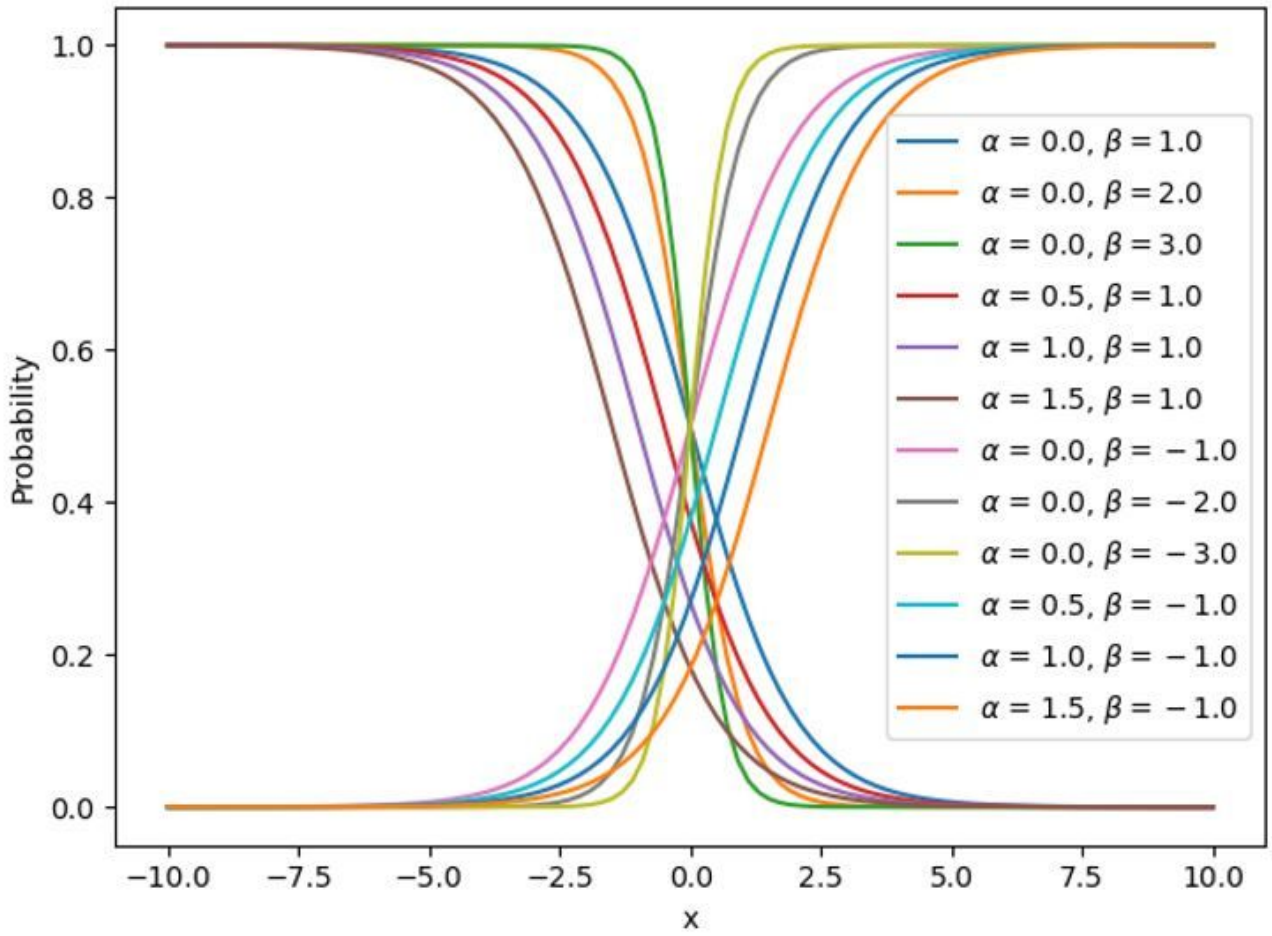

Figure 2

The shape of the LOGISTIC regression function under different parameter combinations

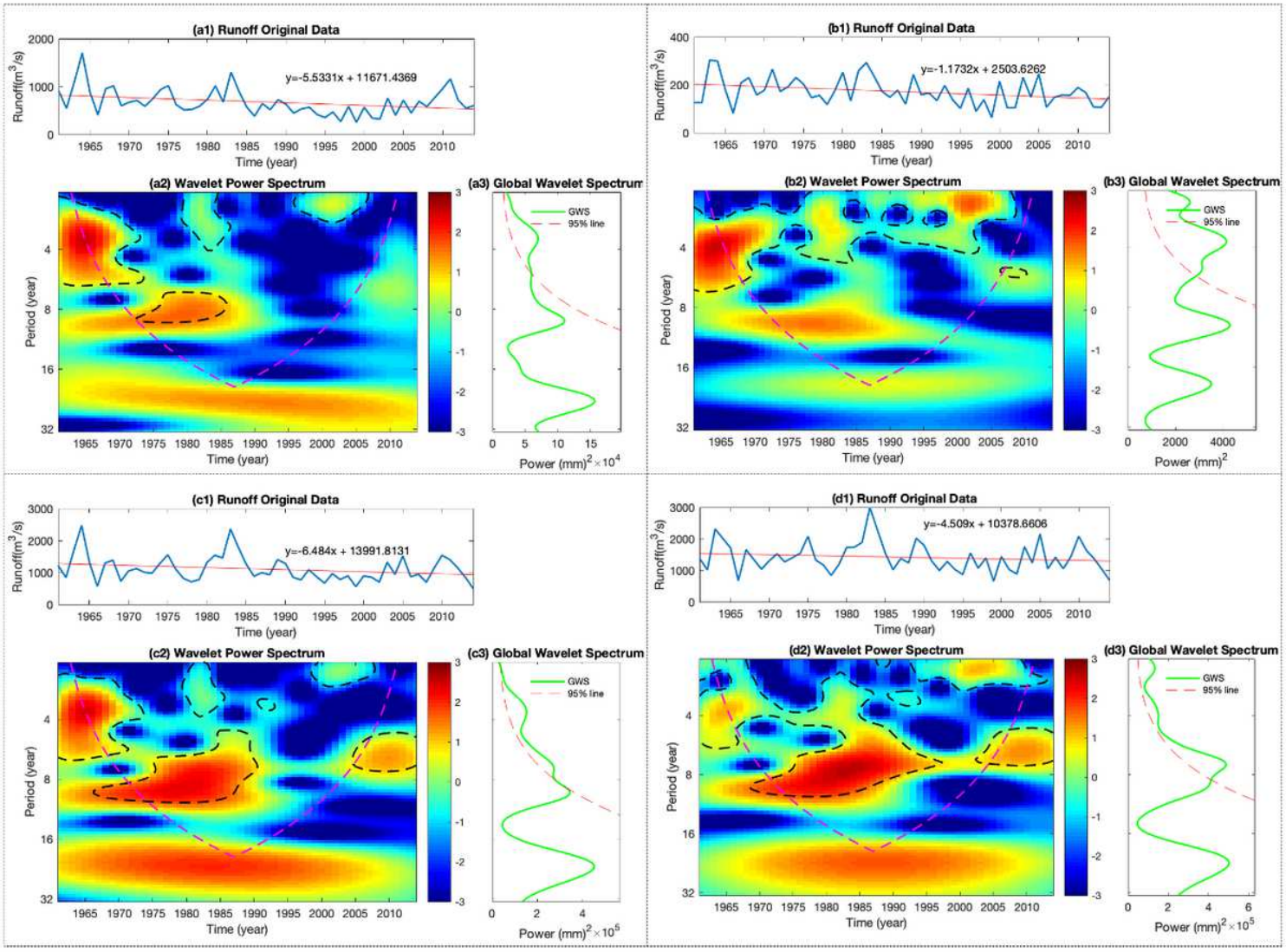

Figure 3

Wavelet power analysis of runoff from four hydrological stations (a: BH, b: HLT, c: HJG, d: HZ)

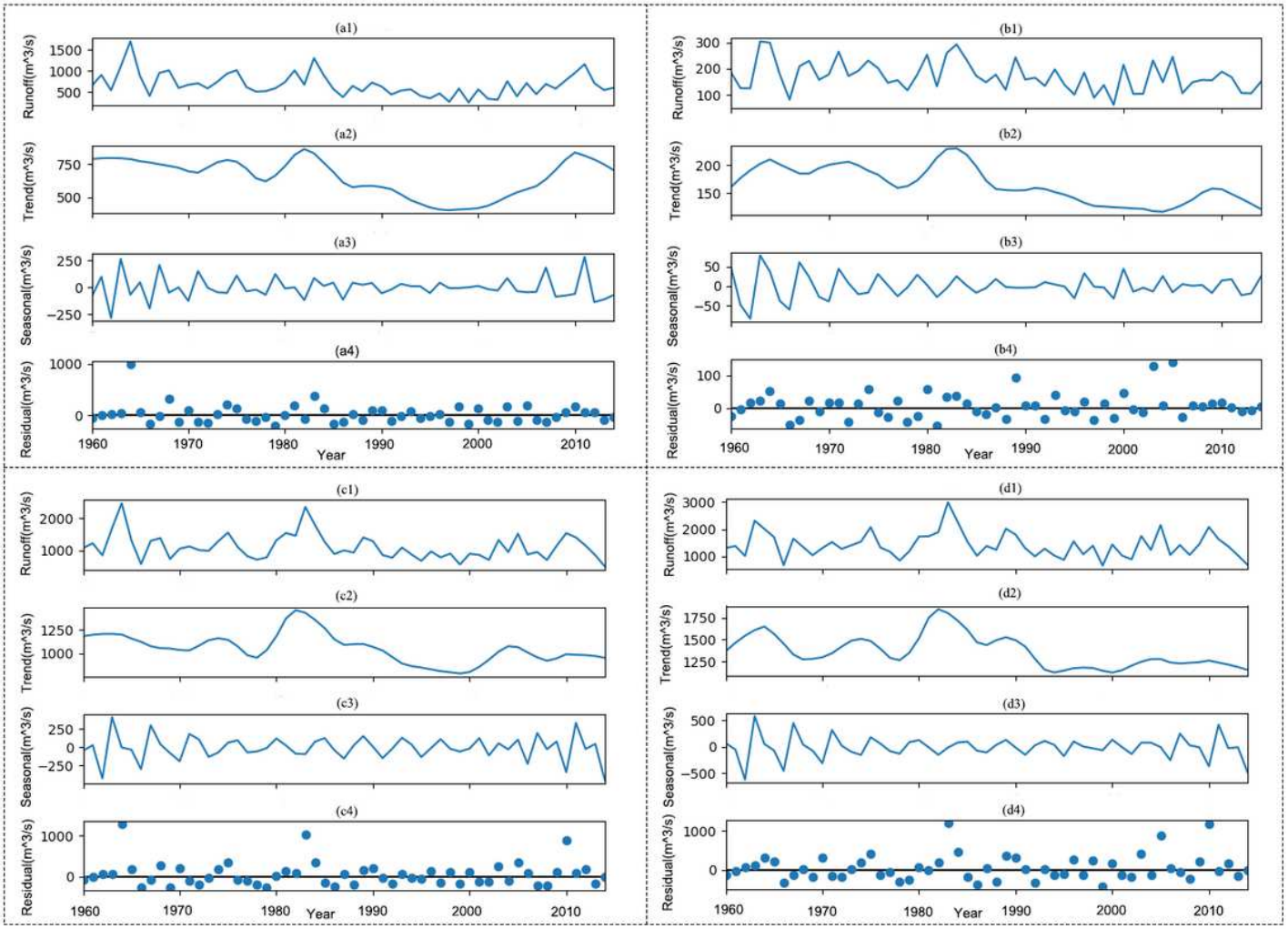

Figure 4

STL decomposition of runoff from four hydrological stations (a: BH, b: HLT, c: HJG, d: HZ)

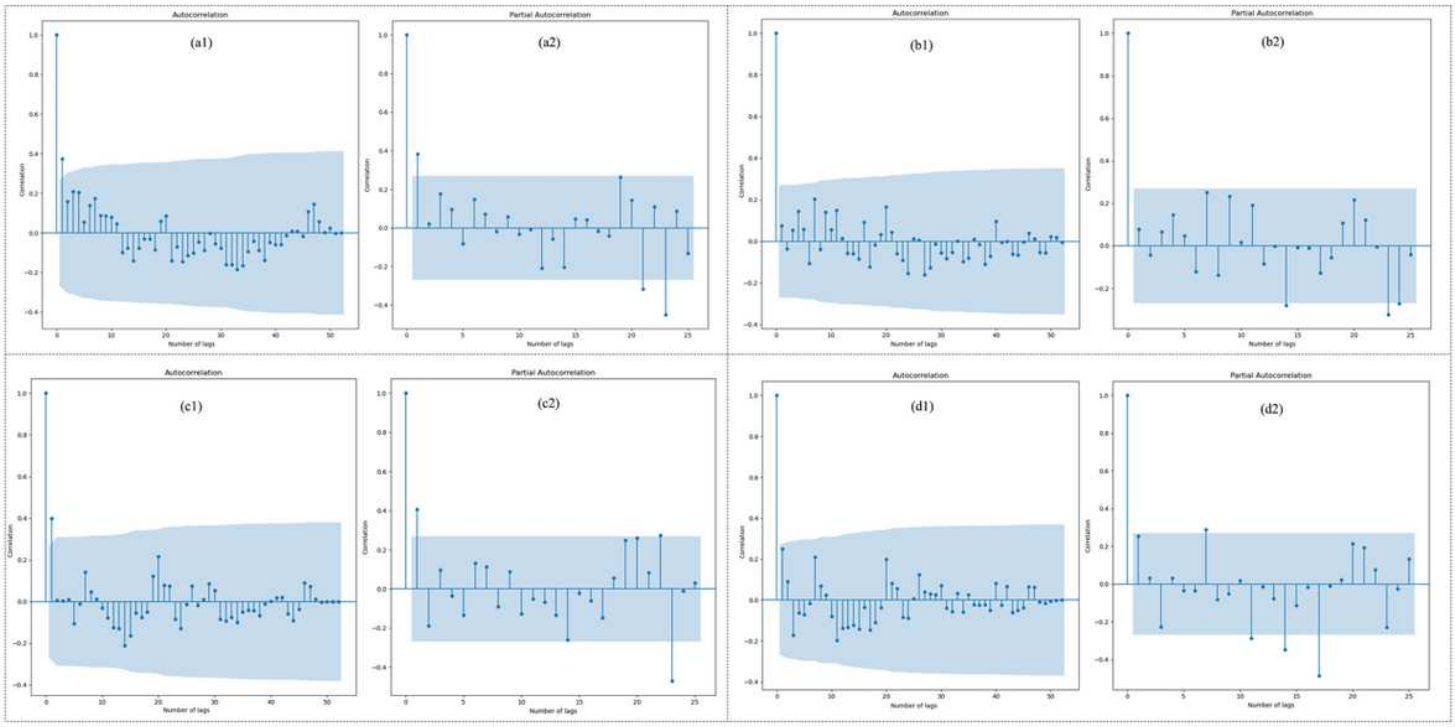

Figure 5

ACF and PACF diagrams of runoff from the four hydrological stations (a: BH, b: HLT, c: HJG, d: HZ)

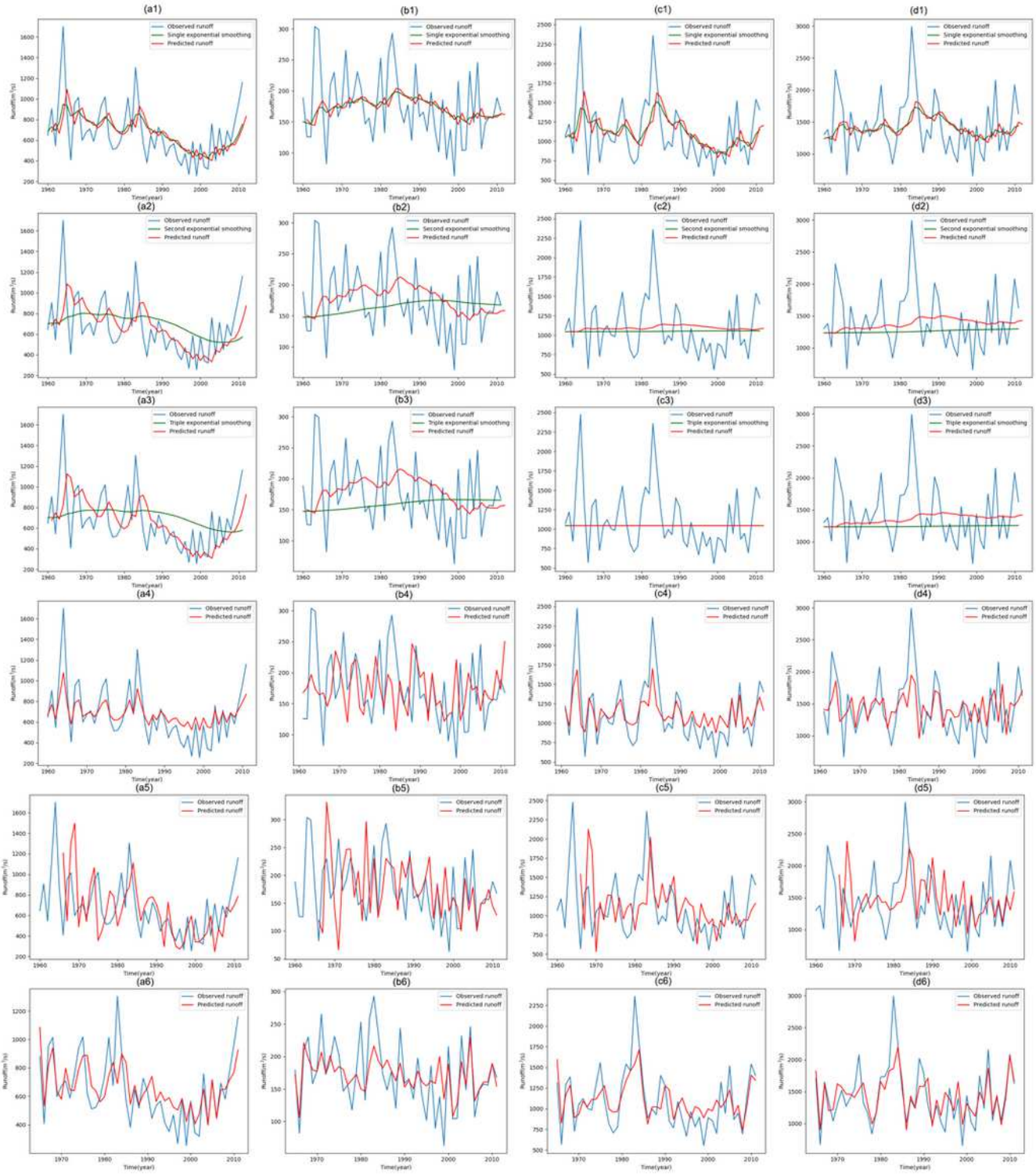

Figure 6

SES, SEES, CES, ARIMA, SARIMA, and DNN simulation results of runoff at the four hydrological stations in calibration period (a: BH, b: HLT, c: HJG, d: HZ)

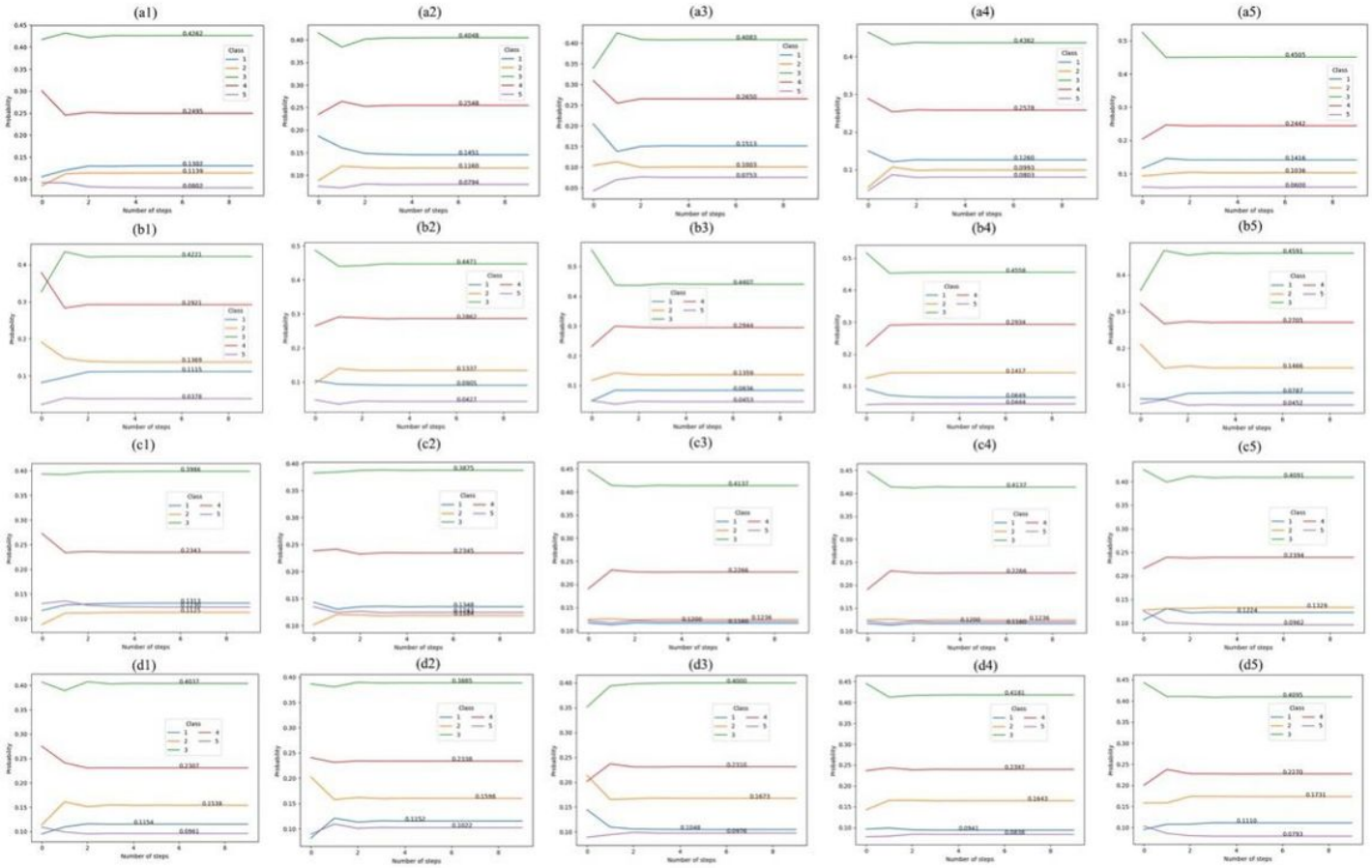

Figure 7

Probability of the five states of runoff from four hydrological stations reaching the stable stage under 1 to 5 steps (a: BH, b: HLT, c: HJG, d: HZ)

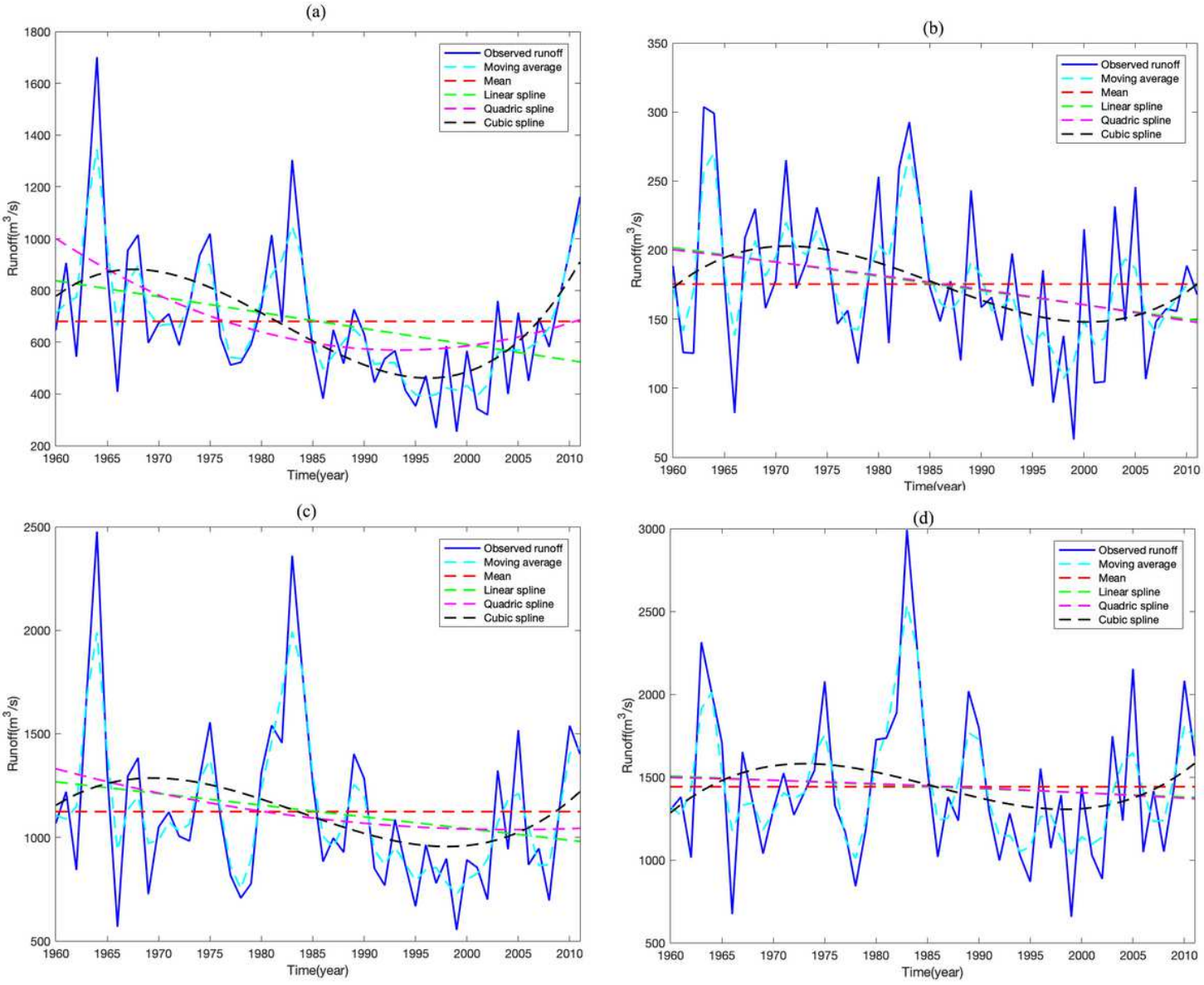

Figure 8

Simulation of runoff process in four hydrological stations with different fitting methods (a: BH, b: HLT, c: HJG, d: HZ)

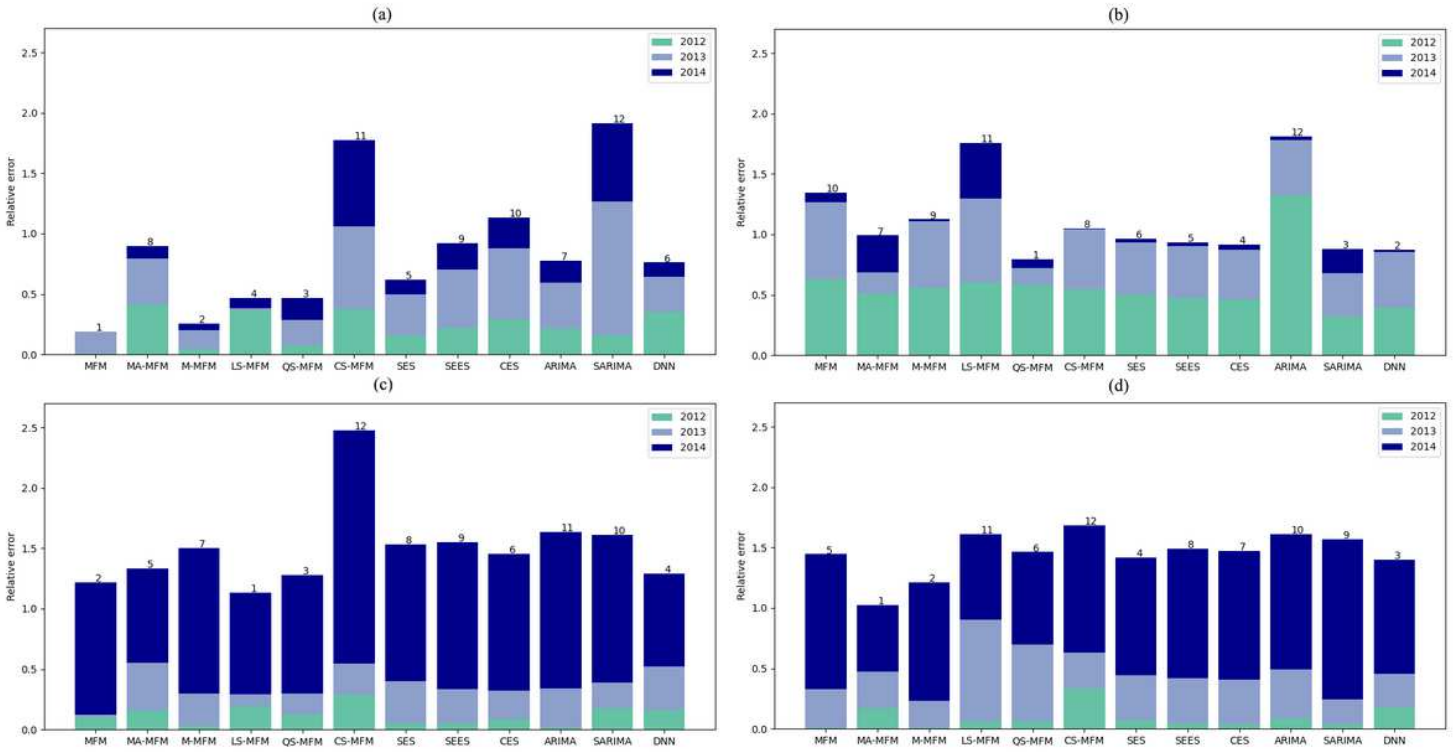

Figure 9

The cumulative relative error results of the runoff simulation of the four hydrological stations during the validation period with different prediction methods (a: BH, b: HLT, c: HJG, d: HZ)

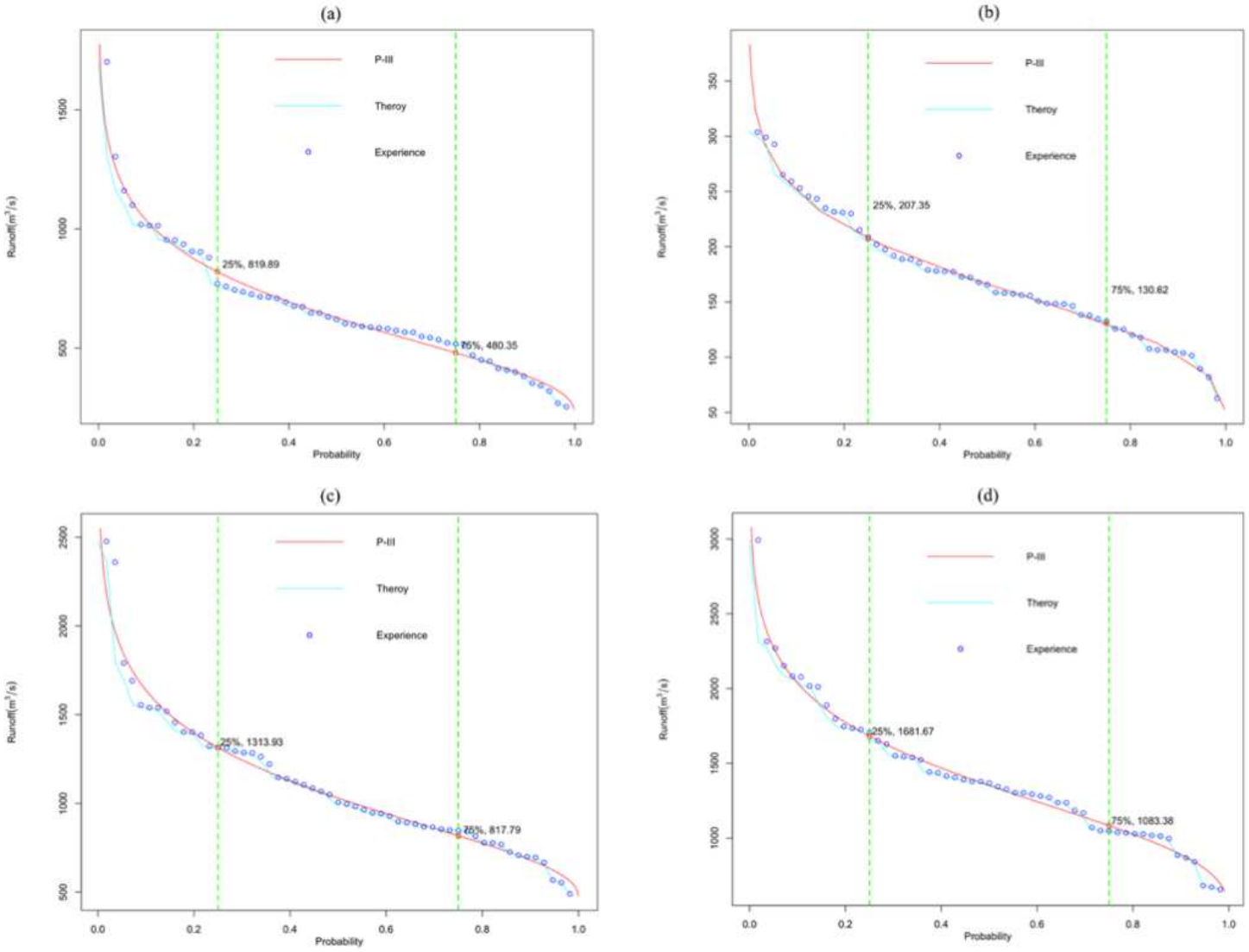

Figure 10

Runoff P-III curve fitting of four hydrological stations (a: BH, b: HLT, c: HJG, d: HZ)

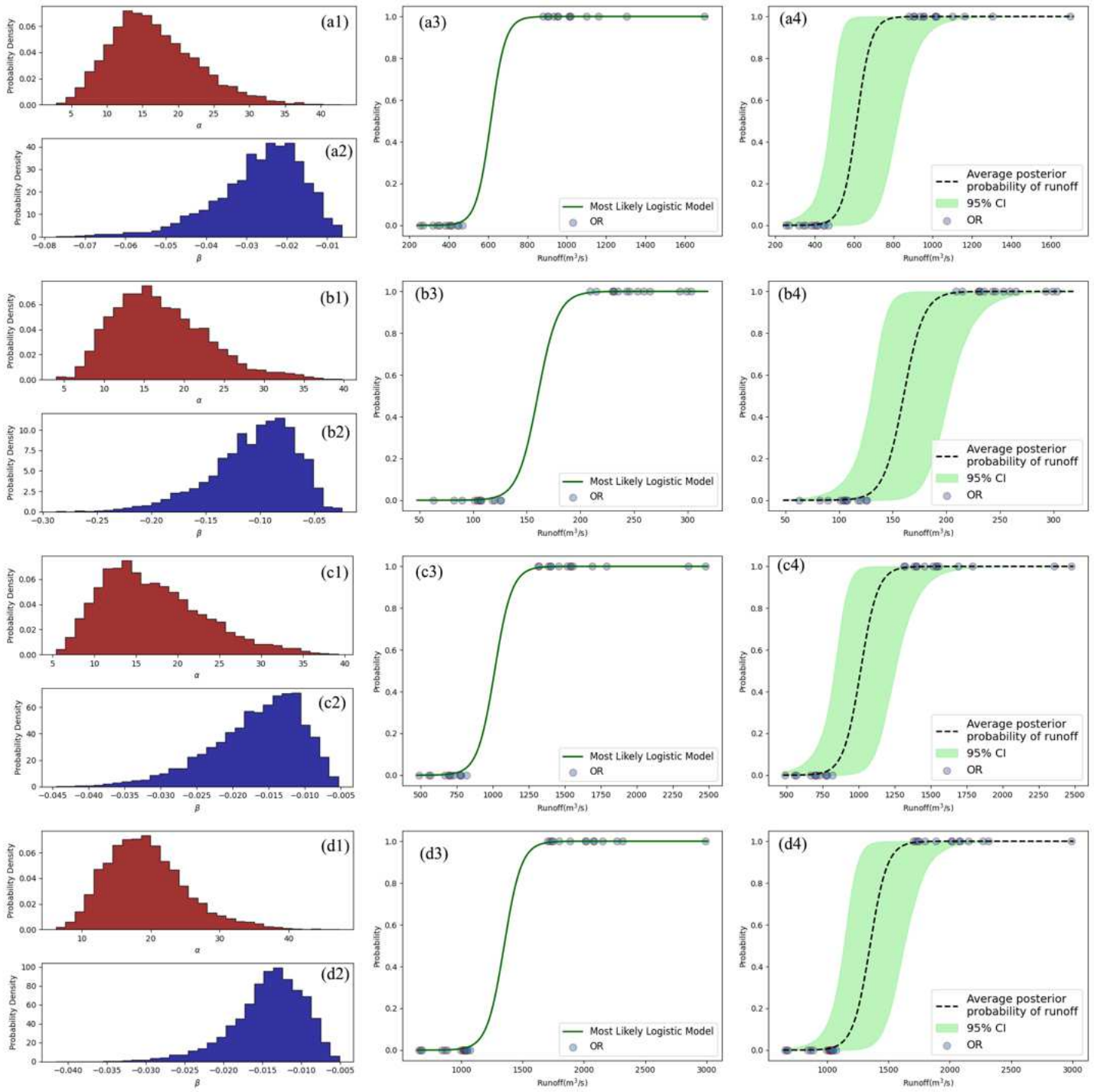

Figure 11

Logistic model parameter selection, model fitting and posterior probability distribution fitting of the four hydrological runoff (a: BH, b: HLT, c: HJG, d: HZ)

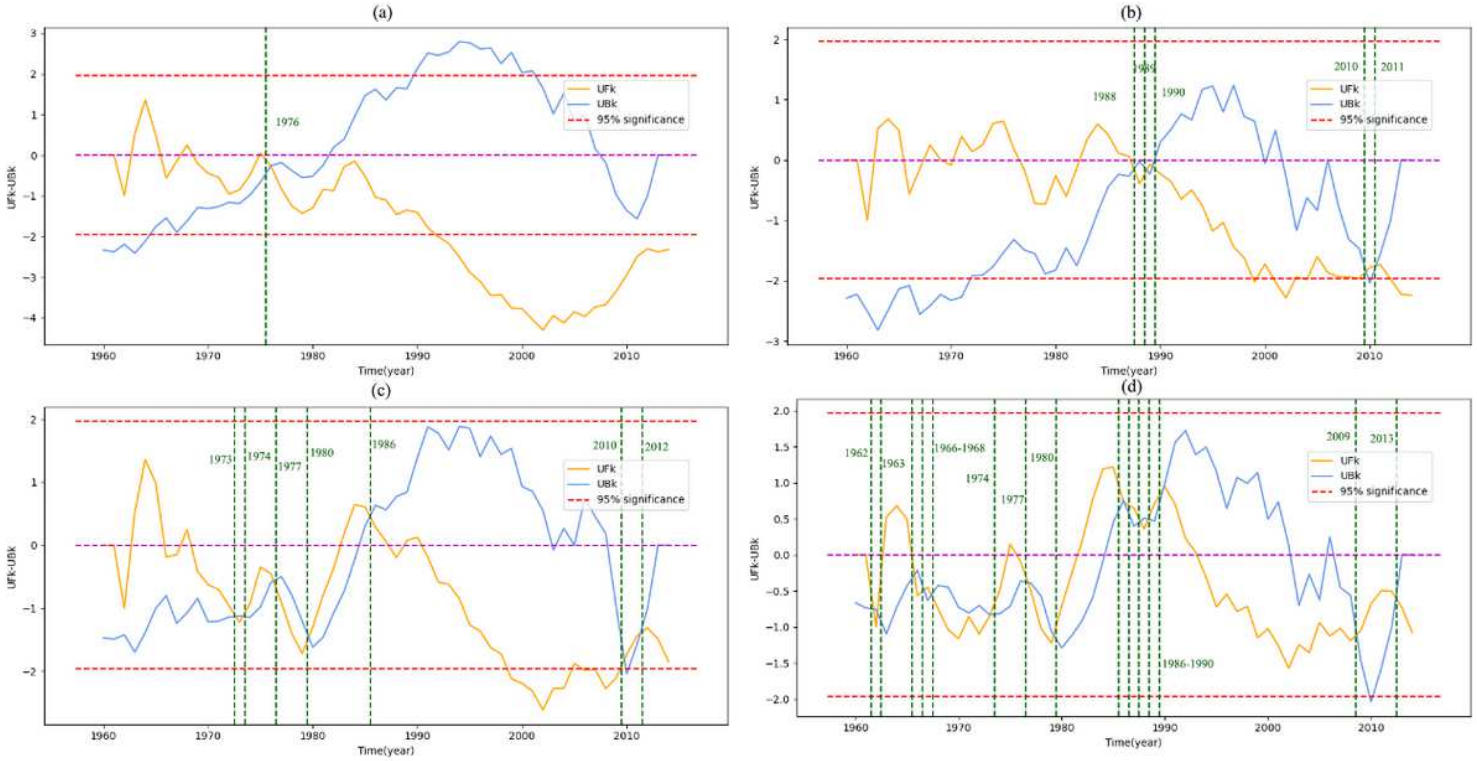

Figure 12

MK trend and mutation test of runoff from four hydrological stations (a: BH, b: HLT, c: HJG, d: HZ)